

Article

Recent Progress in the Viscosity Modeling of Concentrated Suspensions of Unimodal Hard Spheres

Rajinder Pal

Department of Chemical Engineering, University of Waterloo, Waterloo, ON N2L 3G1, Canada; rpal@uwaterloo.ca; Tel.: +1-519-888-4567 (ext. 32985)

Abstract: The viscosity models for concentrated suspensions of unimodal hard spheres published in the twenty-first century are reviewed, compared, and evaluated using a large pool of available experimental data. The Pal viscosity model for unimodal suspensions is the best available model in that the predictions of this model agree very well with the low (zero)-shear experimental relative viscosity data for coarse suspensions, nanosuspensions, and coarse suspensions thickened by starch nanoparticles. The average percentage error in model predictions is less than 6.5%. Finally, the viscous behavior of concentrated multimodal suspensions is simulated using the Pal model for unimodal suspensions.

Keywords: viscosity; relative viscosity; rheology; flow behavior; suspensions; dispersions; viscosity models; particles; nanosuspensions; nanoparticles

1. Introduction

Suspensions of solid particles in a liquid medium are ubiquitous. They form a large group of materials of industrial importance. Both aqueous and non-aqueous suspensions are encountered in industrial applications. Some examples of suspensions are blood, drilling fluid, paint, ink, and a mixture of flour and water. Some of the industries wherein suspensions play a vital role are food, paints, pharmaceutical, mineral processing, coal, ceramics, pulp and paper, polymers, construction, petroleum, agriculture, cosmetics and toiletries, biotechnology, and nanotechnology [1–11].

Understanding the rheological behavior of suspensions is important from both theoretical and practical points of view. The key rheological property of a suspension is its shear viscosity. Knowledge of the shear viscosity of suspensions as a function of particle concentration is required for the design, selection, and operation of the equipment involved in the formulation, mixing, processing, storage, and pipeline transportation of suspensions.

In this article, the recent progress made in the viscosity modeling of concentrated suspensions is reviewed. The key viscosity models for suspensions published in the twenty-first century are discussed and compared. The available models are also evaluated using a large pool of low (zero)-shear experimental viscosity data available on coarse suspensions, nanosuspensions, and coarse suspensions thickened by starch nanoparticles (SNPs).

2. Theoretical Background

2.1. Dilute Suspensions of Hard Spheres

For a dilute suspension of identical hard-sphere-type particles, the rheological constitutive equation is given as follows [1,12]:

$$\bar{\sigma} = -P\bar{\delta} + 2\eta_m\bar{E} + \frac{3\varphi}{4\pi R^3}\bar{S}^0 \quad (1)$$

where \bar{S}^0 is the dipole strength of a single hard-sphere particle located in an infinite matrix fluid, φ is the volume fraction of particles, R is the particle radius, \bar{E} is the bulk rate of the



Citation: Pal, R. Recent Progress in the Viscosity Modeling of Concentrated Suspensions of Unimodal Hard Spheres. *ChemEngineering* **2023**, *7*, 70. <https://doi.org/10.3390/chemengineering7040070>

Academic Editors: George Z. Papageorgiou and José P. Coelho

Received: 2 July 2023

Revised: 21 July 2023

Accepted: 26 July 2023

Published: 27 July 2023



Copyright: © 2023 by the author. Licensee MDPI, Basel, Switzerland. This article is an open access article distributed under the terms and conditions of the Creative Commons Attribution (CC BY) license (<https://creativecommons.org/licenses/by/4.0/>).

strain tensor, η_m is the matrix viscosity, P is the average pressure, $\bar{\delta}$ is a unit tensor, and $\bar{\sigma}$ is the bulk (average) stress tensor.

The dipole strength of a single hard-sphere particle located in an infinite matrix fluid, \bar{S}^0 , is given as follows:

$$\bar{S}^0 = \frac{20}{3} \pi R^3 \eta_m \bar{E}_\infty \quad (2)$$

where \bar{E}_∞ is the rate of the strain tensor far away from the sphere. The rate of the strain tensor, \bar{E}_∞ , far away from the particles in dilute suspensions can be equated to the bulk or imposed rate of the strain tensor, \bar{E} , on the suspension. Upon substitution of \bar{S}^0 from Equation (2) into Equation (1), we obtain the following:

$$\bar{\sigma} = -P \bar{\delta} + 2\eta_m \left(1 + \frac{5}{2}\varphi\right) \bar{E} \quad (3)$$

For a homogeneous incompressible Newtonian fluid possessing a shear viscosity, η , the constitutive equation is given as follows:

$$\bar{\sigma} = -P \bar{\delta} + 2\eta \bar{E} \quad (4)$$

Upon comparison of Equations (3) and (4), the following expression for the viscosity of a dilute suspension of solid hard-sphere-type particles is obtained:

$$\eta = \eta_m \left(1 + \frac{5}{2}\varphi\right) \quad (5)$$

This is the celebrated Einstein equation [13,14] for the viscosity of a dilute suspension of hard-sphere-type solid particles. The Einstein equation was published in 1906 (erratum published in 1911).

Batchelor [15] extended the Einstein relationship, as in Equation (5), to the second order as follows:

$$\eta = \eta_m \left(1 + \frac{5}{2}\varphi + B\varphi^2\right) \quad (6)$$

where $B = 6.2$ for Brownian suspensions at a low Peclet number. However, this equation gives reasonable predictions of suspension viscosity only at particle concentrations lower than about 15 vol%. At higher particle concentrations, the experimental values of viscosity generally fall well above the predictions of this equation, and the gap increases with an increase in particle concentration.

A number of numerical simulation studies have been published to extend the work of Einstein to higher concentrations by taking into account the hydrodynamic and nonhydrodynamic interactions between particles [16–18]. For example, Ladd [17] determined the relative viscosity of random suspensions of hard spheres from a multipole-moment expansion of force density on the surface of solid particles. Based on his numerical simulation results, Ladd developed the following expression for the high-frequency relative viscosity of a suspension:

$$\frac{\eta - \eta_m}{\eta - (3/2)\eta_m} = \varphi \left(1 + \varphi + \varphi^2 - 2.3\varphi^3\right) \quad (7)$$

In the limit $\varphi \rightarrow 0$, the Ladd expression reduces to the Einstein equation. Although the Ladd expression is applicable over a somewhat broader range of φ , as compared with the Einstein equation, it too fails to give accurate predictions of relative viscosity at particle concentrations larger than about 15 vol%. Also, note that this equation is restricted to suspensions subject to only hydrodynamic interactions.

2.2. Concentrated Suspensions of Hard Spheres

The publication of the Einstein equation triggered a lot of long-lasting activity on the rheology of dilute and concentrated suspensions [19–72]. In this section, two well-known models for the viscosity of concentrated suspensions are discussed, namely, the Mooney model [24] and the Krieger–Dougherty model [34]. These models are applicable over the full range of particle concentrations, ranging from zero to packed-bed concentrations.

Consider a suspension with a volume fraction of particles, φ_1 . The relative viscosity of this suspension can be expressed as follows:

$$\eta_r = \frac{\eta}{\eta_m} = H(\varphi_1) \quad (8)$$

where $H(\varphi_1)$ is the relative viscosity function. In the limit $\varphi \rightarrow 0$, $H(\varphi_1)$ is given by the Einstein equation, as in Equation (5), as follows:

$$H(\varphi_1) = 1 + 2.5\varphi_1 \quad (9)$$

We now add more particles to the existing suspension of a concentration φ_1 such that the new concentration of the suspension is $\varphi_1 + \varphi_2$. Treating the previous suspension as a continuous phase (matrix) with respect to the new particles, we can write the following:

$$\eta_r(\varphi_2) = \frac{\eta(\varphi_1 + \varphi_2)}{\eta(\varphi_1)} = H(\varphi_2) = \frac{H(\varphi_1 + \varphi_2)}{H(\varphi_1)} \quad (10)$$

Thus:

$$H(\varphi_1 + \varphi_2) = H(\varphi_1)H(\varphi_2) \quad (11)$$

This functional relationship does not consider the crowding effect of particles. Mooney proposed the following functional relation for concentrated suspensions taking into consideration the crowding effect of particles:

$$H(\varphi_1 + \varphi_2) = H\left(\frac{\varphi_1}{1 - \varphi_2/\varphi_m}\right)H\left(\frac{\varphi_2}{1 - \varphi_1/\varphi_m}\right) \quad (12)$$

where φ_m is the maximum packing volume fraction of particles. This functional relationship gives the following solution for the relative viscosity of a concentrated suspension with any volume fraction, φ , which also satisfies the Einstein equation in the limit $\varphi \rightarrow 0$:

$$\eta_r = H(\varphi) = \exp\left(\frac{2.5\varphi}{1 - \varphi/\varphi_m}\right) \quad (13)$$

This is the celebrated Mooney equation for the viscosity of unimodal concentrated suspensions of spherical particles. The Mooney equation was published in 1951 [24].

According to Krieger and Dougherty [34], Equation (13) over-corrects the crowding and packing of particles. They proposed a modified version of the functional relationship, as in Equation (12), as follows:

$$H(\varphi_1 + \varphi_2) = H(\varphi_1)H\left(\frac{\varphi_2}{1 - \varphi_1/\varphi_m}\right) \quad (14)$$

This equation considers the crowding effect for only the second fraction of particles added to the suspension. The solution of Equation (14), which also satisfies the Einstein equation in the limit $\varphi \rightarrow 0$, is given as follows:

$$\eta_r = H(\varphi) = \left(1 - \frac{\varphi}{\varphi_m}\right)^{-2.5\varphi_m} \quad (15)$$

This is the celebrated Krieger–Dougherty equation for the viscosity of unimodal concentrated suspensions of spherical particles. The Krieger–Dougherty equation was published in 1959 [34].

The Mooney and Krieger–Dougherty equations are used extensively in the literature to describe the viscosity data of concentrated suspensions subject to hydrodynamic and Brownian interactions. They both diverge in the limit $\varphi \rightarrow \varphi_m$. The maximum packing volume fraction of unimodal suspensions usually falls in a range of $0.58 \leq \varphi_m \leq 0.64$. A φ_m of 0.58 corresponds to the glass transition (GT) point of a suspension, and a φ_m of 0.64 corresponds to random close packing (RCP) of uniform spherical particles.

3. Recent Progress in the Viscosity Modeling of Concentrated Suspensions

Many articles have been published on the development of viscosity models for concentrated suspensions in the twentieth century [20,23–28,31,32,34–41,44,45,50]. A good number of review articles have also been published on the subject [35,43]. Among the most popular models published in the twentieth century for the viscosity of concentrated suspensions are the Mooney and Krieger–Dougherty models discussed in the preceding section. In what follows, the relative viscosity models for concentrated suspensions published recently, in the past decade or so, are reviewed, compared, and evaluated using a large pool of experimental viscosity data available for concentrated suspensions.

3.1. Cheng et al. Model (2002)

Cheng et al. [73] proposed the following theoretical model for the low-shear viscosity of concentrated colloidal suspensions of hard spheres:

$$\eta_r = \eta_{r\infty} + \Delta\eta_o \quad (16)$$

where $\eta_{r\infty}$ is the high-frequency hydrodynamic contribution and $\Delta\eta_o$ is the non-hydrodynamic contribution to the relative viscosity of a suspension. The high-frequency relative viscosity is given by the following equations:

$$\eta_{r\infty} = \frac{1 + \frac{3}{2}[1 + \varphi(1 + \varphi - 2.3\varphi^2)]}{1 - \varphi[1 + \varphi(1 + \varphi - 2.3\varphi^2)]} \quad 0 \leq \varphi \leq 0.56 \quad (17)$$

$$\eta_{r\infty} = 15.78 \ln\left(\frac{1}{1 - 1.16\varphi^{1/3}}\right) - 42.47 \quad 0.60 \leq \varphi < 0.64 \quad (18)$$

The non-hydrodynamic contribution to the relative viscosity of the suspension is given as follows:

$$\Delta\eta_o = 0.20 \exp\left(\frac{0.60}{\varphi_m - \varphi}\right) \quad (19)$$

3.2. Mendoza and Santamaria-Holek Model (2009)

Mendoza and Santamaria-Holek [63] modified the following Roscoe–Brinkman model for the viscosity of moderately concentrated suspensions of hard-sphere-type particles:

$$\eta_r = H(\varphi) = (1 - \varphi)^{-2.5} \quad (20)$$

where $H(\varphi)$ is the relative viscosity–concentration function of a suspension. They replaced the actual volume fraction of particles, φ , with an effective volume fraction, φ_{eff} , defined as follow:

$$\varphi_{eff} = \frac{\varphi}{1 - c\varphi} \quad (21)$$

where c is given as follows:

$$c = \frac{1 - \varphi_m}{\varphi_m} \quad (22)$$

Thus, the viscosity model of Mendoza and Santamaria-Holek is given as follows:

$$\eta_r = H(\varphi) = \left(1 - \frac{\varphi}{1 - c\varphi}\right)^{-2.5} \quad (23)$$

In the limit $\varphi \rightarrow 0$, this model reduces to the Einstein equation; in the limit $\varphi \rightarrow \varphi_m$, the viscosity diverges.

3.3. Brouwers Model (2010)

Based on geometrical considerations, Brouwers [64] developed the following differential equation for the relative viscosity of a concentrated suspension of unimodal hard spheres:

$$\frac{2.5H(\varphi)}{(1 - \varphi)(1 - \frac{\varphi}{\varphi_m})} = \frac{dH}{d\varphi} \quad (24)$$

Upon integration and application of the boundary condition, $H(\varphi = 0) = 1$, the differential equation, as in Equation (24), gives the following solution:

$$\eta_r = H(\varphi) = \left(\frac{1 - \varphi}{1 - \frac{\varphi}{\varphi_m}}\right)^{2.5\varphi_m/(1 - \varphi_m)} \quad (25)$$

This equation, referred to as Brouwers model, can also be rearranged as follows:

$$\eta_r = H(\varphi) = \left[1 - \left(\frac{1 - \varphi_m}{\varphi_m}\right) \left(\frac{\varphi}{1 - \varphi}\right)\right]^{-2.5\varphi_m/(1 - \varphi_m)} \quad (26)$$

The Brouwers model reduces to the Einstein equation in the limit $\varphi \rightarrow 0$. Also, it diverges in the limit $\varphi \rightarrow \varphi_m$.

3.4. Faroughi–Huber Model (2015)

Faroughi and Huber [70] used a differential effective medium approach similar to that used by Pal [60,69] to obtain the following differential equation:

$$\frac{d\eta}{\eta} = 2.5 \left(\frac{d\varphi'}{1 - \Omega\varphi'}\right) \quad (27)$$

where $\varphi' = \varphi/(1 - \varphi)$, and Ω is a self-crowding parameter given as follows:

$$\Omega = \frac{1 - \varphi_m}{\varphi_m} \quad (28)$$

Note that Ω is equal to c of the Mendoza and Santamaria-Holek model (see Equation (22)).

Upon integration, Equation (27) yields the following expression:

$$\eta_r = H(\varphi) = \left[1 - \Omega \left(\frac{\varphi}{1 - \varphi}\right)\right]^{-2.5/\Omega} \quad (29)$$

It is important to note that this model proposed in the Faroughi and Huber [70] article is not original. It is identical to the Brouwers model, as shown in Equation (26). Upon substitution of Ω from Equation (28) into Equation (29), Equation (29) reduces to the following Brouwers model:

$$\eta_r = H(\varphi) = \left[1 - \left(\frac{1 - \varphi_m}{\varphi_m}\right) \left(\frac{\varphi}{1 - \varphi}\right)\right]^{-2.5\varphi_m/(1 - \varphi_m)}$$

Surprisingly, the authors claim this to be their own model, not recognizing that it is an exact replica of the Brouwers model.

3.5. Pal Model (2015)

Pal [69] proposed a model for the viscosity of concentrated suspensions considering the clustering of particles. The clustering of particles is expected with an increase in particle concentration. Due to Brownian motion, particles encounter each other and form clusters. Even in the absence of Brownian motion, the clustering of particles is expected under the application of shearing motion. Particles are known to form clusters that are continually created and destroyed in shearing motion [46]. At low concentrations of particles, clusters may consist of just doublets. The size of clusters grows progressively from doublets to triplets, from triplets to quartets, from quartets to quintets, and so on. The clustering process is shown schematically in Figure 1 as the concentration of particles is increased. Due to the clustering of particles, a significant amount of the continuous phase is immobilized within the clusters, resulting in an increase in the effective volume fraction of the dispersed phase. Based on the general characteristics of suspensions of solid particles, Pal proposed the following relationship between the effective dispersed-phase concentration (φ_{eff}) of a suspension and the actual dispersed-phase concentration (φ) [69]:

$$\varphi_{eff} = \left[1 + \left(\frac{1 - \varphi_m}{\varphi_m} \right) \left(\sqrt{1 - \left(\frac{\varphi_m - \varphi}{\varphi_m} \right)^2} \right) \right] \varphi \quad (30)$$

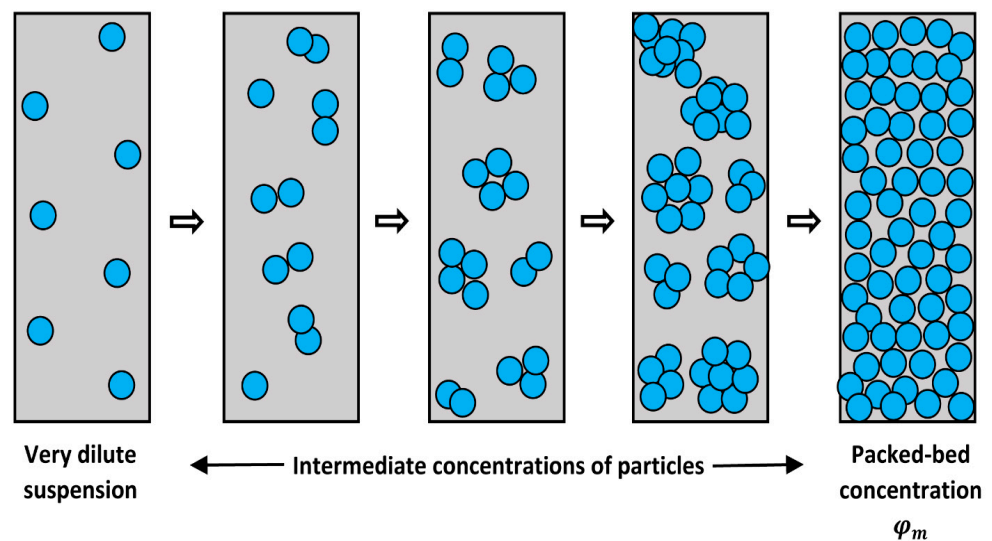


Figure 1. Clustering of particles with an increase in particle concentration.

The important features of this expression are as follows:

- (a) In the dilute limit $\varphi \rightarrow 0$, $\varphi_{eff} = \varphi$;
- (b) In the limit $\varphi \rightarrow \varphi_m$, $\varphi_{eff} = 1$;
- (c) The slope of the ratio, φ_{eff}/φ , with respect to φ , is always positive, that is, $\partial(\varphi_{eff}/\varphi)/\partial\varphi \geq 0$. The ratio, φ_{eff}/φ , is expected to only increase with an increase in φ due to an increase in the size of clusters.

(d) The ratio, φ_{eff}/φ , becomes constant at high values of φ . This ratio does not continue to increase with an increase in the number of particles in clusters. When the number of particles in a cluster has reached a certain value, the ratio, φ_{eff}/φ , is expected to become constant. For clusters with a large number of particles, the ratio, φ_{eff}/φ , depends only on the type of particle packing (random close packing, hexagonal close packing, etc.).

Thus, $\partial(\varphi_{eff}/\varphi)/\partial\varphi = 0$ in the limit $\varphi \rightarrow \varphi_m$.

Figure 2 shows the plots of φ_{eff}/φ versus φ generated from Equation (30) for two different types of particle packing clusters, namely, random close packing (RCP) and glass transition (GT) packing of particles. Note that $\varphi_m = 0.637$ for random close packing and $\varphi_m = 0.58$ for glass transition packing of uniform spheres. The ratio, φ_{eff}/φ , increases initially with an increase in φ but levels off at high values of φ . The ratio, φ_{eff}/φ , becomes equal to $1/\varphi_m$ as $\varphi \rightarrow \varphi_m$, that is, φ_{eff} reaches a value of unity.

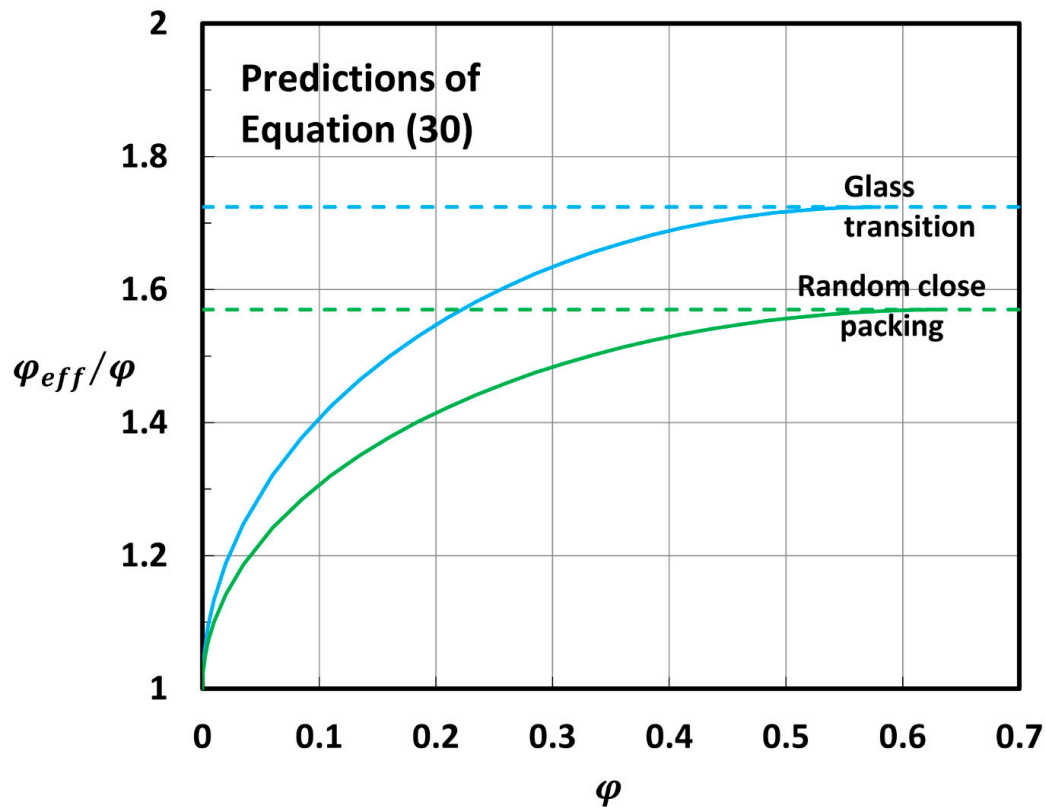


Figure 2. Increase in φ_{eff}/φ with an increase in φ for two different types of particle packing clusters.

The viscosity model for concentrated suspensions was derived using a differential effective medium approach. In this approach, it is visualized that a concentrated suspension can be obtained from the starting suspending medium by successively adding differential quantities of particles to the suspension until the final concentration of particles is obtained. Let, at any stage (i) in the process of particle addition, the total volume of the suspension be V_t , the effective dispersed-phase volume be V_e , and the viscosity of suspension be η . Upon addition of dV_d of the dispersed phase to the stage (i) suspension, the stage (i + 1) is reached where the effective dispersed-phase volume is $V_e + dV_e$, the total volume of the suspension is $V_t + dV_d$, and the viscosity of the suspension is $\eta + d\eta$. Treating the stage (i) suspension as an effective medium of viscosity, η , with respect to the stage (i + 1) suspension of viscosity, $\eta + d\eta$, the application of the Einstein equation gives the following:

$$\eta + d\eta = \eta \left[1 + 2.5 \left(\frac{dV_e}{V_t + dV_d} \right) \right] \quad (31)$$

It can be readily shown that:

$$\frac{dV_e}{V_t + dV_d} = \frac{d\varphi_{eff}}{1 - \varphi_{eff}} \quad (32)$$

From Equations (31) and (32), it follows that:

$$\frac{d\eta}{\eta} = 2.5 \left(\frac{d\varphi_{eff}}{1 - \varphi_{eff}} \right) \quad (33)$$

The integration of Equation (33) yields the following expression:

$$\eta_r = \frac{\eta}{\eta_c} = (1 - \varphi_{eff})^{-2.5} \quad (34)$$

Upon substitution of Equation (30) into Equation (34), the following model for the viscosity of concentrated suspensions of unimodal spherical particles is obtained:

$$\eta_r = H(\varphi) = \left[1 - \left\{ 1 + \left(\frac{1 - \varphi_m}{\varphi_m} \right) \sqrt{1 - \left(\frac{\varphi_m - \varphi}{\varphi_m} \right)^2} \right\} \varphi \right]^{-2.5} \quad (35)$$

This model is referred to as Pal model P1 in the remainder of this article.

3.6. Pal Model (2017)

Starting from the Einstein equation, as in Equation (5), Pal [71] proposed a new model for the viscosity of concentrated suspensions of hard spheres. According to the Einstein equation, as in Equation (5):

$$\eta_r = 1 + \frac{5}{2} \left(\frac{\text{Volume of particles}}{\text{Volume of suspension}} \right) \quad (36)$$

In analogy with real gas behavior, Pal [71] modified the Einstein equation as follows:

$$\eta_r = 1 + \frac{5}{2} \left(\frac{\text{Volume of particles}}{\text{Free volume available to particles}} \right) \quad (37)$$

Pal contended that the volume of particles should be excluded from the total volume of the suspension in the calculation of the particle concentration.

Let V_t be the total volume of suspension and φ be the volume fraction of particles. Thus, the following can be expressed:

$$\begin{aligned} \text{Free volume available to particles} &= \text{Total volume of suspension} - \\ \text{Volume of particles} &= V_t - \varphi V_t \end{aligned} \quad (38)$$

From Equations (37) and (38), we obtain:

$$\eta_r = 1 + \frac{5}{2} \left(\frac{\varphi V_t}{V_t - \varphi V_t} \right) = 1 + \frac{5}{2} \left(\frac{\varphi}{1 - \varphi} \right) \quad (39)$$

Pal [71] further modified this equation taking into consideration the clustering of particles. Thus, the actual volume fraction of particles in Equation (39) was replaced by an effective volume fraction, φ_{eff} , given as follows (see Equation (30)):

$$\frac{\varphi_{eff}}{\varphi} = 1 + \left(\frac{1 - \varphi_m}{\varphi_m} \right) \left[\sqrt{1 - \left(\frac{\varphi_m - \varphi}{\varphi_m} \right)^2} \right] \quad (40)$$

Consequently, the viscosity model for a concentrated suspension of hard spheres as proposed by Pal [71] is as follows:

$$\eta_r = 1 + \frac{5}{2} \left(\frac{\varphi_{eff}}{1 - \varphi_{eff}} \right) \quad (41)$$

where φ_{eff} is given by Equation (40). This model is referred to as Pal model P2 in the remainder of this article.

3.7. Pal Model (2020)

Pal [72] recently developed another suspension viscosity model for non-dilute suspensions. Considering the clustering of particles in shear flow, he proposed a linear relationship between the aggregation coefficient and volume fraction of particles:

$$k = a + b\varphi \quad (42)$$

where k is the aggregation coefficient defined as follows:

$$k = \frac{\varphi_{eff}}{\varphi} \quad (43)$$

Applying the following conditions: $k = 1$ when $\varphi \rightarrow 0$ and $k = 1/\varphi_m$ when $\varphi \rightarrow \varphi_m$ (note that $\varphi_{eff} = 1$ when $\varphi \rightarrow \varphi_m$), the constants a and b can be determined as follows: $a = 1$ and $b = (1 - \varphi_m)/\varphi_m^2$. Thus, the aggregation coefficient and φ_{eff} in shear flow can be expressed as:

$$k = 1 + \left[\frac{1 - \varphi_m}{\varphi_m^2} \right] \varphi \quad (44)$$

$$\varphi_{eff} = \left\{ 1 + \left[\frac{1 - \varphi_m}{\varphi_m^2} \right] \varphi \right\} \varphi \quad (45)$$

This expression for φ_{eff} is simpler than the one developed earlier for Pal model P2 (see Equation (40)). Using the effective medium approach discussed in Section 3.5 and the above expression for φ_{eff} , the following model for concentrated suspensions of unimodal spherical particles was derived:

$$\eta_r = \left[1 - \left\{ 1 + \left(\frac{1 - \varphi_m}{\varphi_m^2} \right) \varphi \right\} \varphi \right]^{-2.5} \quad (46)$$

This model is referred to as Pal model P3 in the remainder of this article.

4. Comparisons of Model Predictions

Figure 3 compares the predictions of various models for two different values of the maximum packing concentration: $\varphi_m^{RCP} = 0.637$ and $\varphi_m^{GT} = 0.58$. The comparisons reveal the following information:

- The Mooney model (M) generally predicts the highest values of relative viscosities.
- Pal model P2 generally predicts the lowest values of relative viscosities.
- The Krieger–Dougherty model (KD) and Pal model P2 predict similar values of relative viscosities.
- The Mendoza and Santamaria-Holek model (MS) generally predicts relative viscosities lower than that of Pal model P3.
- The Cheng et al. (C) model predicts unrealistically high values of relative viscosities when $\varphi < 0.25$. Also, the relative viscosity is greater than unity at $\varphi = 0$.
- For large values of particle volume fractions ($\varphi > 0.50$), the predictions of the models are generally in the following order: $M > C > B > P1 > P3 > MS > KD > P2$.

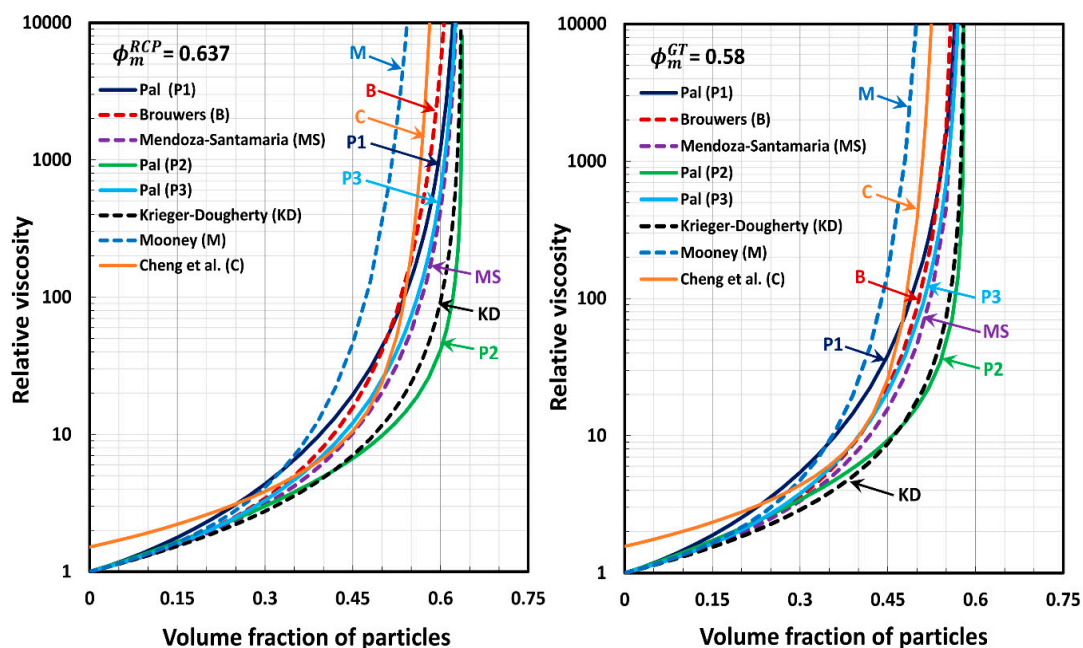


Figure 3. Comparisons of model predictions for two different values of maximum packing concentrations: $\phi_m^{RCP} = 0.637$ and $\phi_m^{GT} = 0.58$. M refers to Mooney model (Equation (13)), C refers to Cheng et al. model (Equation (16)), B refers to Brouwers model (Equation (26)), P1 refers to Pal model P1 (Equation (35)), P2 refers to Pal model P2 (Equation (41)), P3 refers to Pal model P3 (Equation (46)), MS refers to Mendoza and Santamaria-Holek model (Equation (23)), and KD refers to Krieger–Dougherty model (Equation (15)).

5. Comparisons of Model Predictions with Experimental Data

5.1. Experimental Data

The models were evaluated using three groups of low-shear experimental data: coarse suspensions (22 sets of data), nanosuspensions (16 sets of data), and coarse suspensions thickened by starch nanoparticles (6 sets of data). Tables 1–3 give details of these suspensions. The suspensions were unimodal, and the matrix phase of the suspensions was Newtonian. Both Newtonian and non-Newtonian suspensions were considered. For non-Newtonian suspensions, the viscosity data at low-shear rates were used. For some non-Newtonian suspensions that followed power law behavior, a consistency index was used instead of viscosity. Note that a consistency index is equal to viscosity at a low shear rate of 1 s^{-1} . While coarse suspensions were subject to mainly hydrodynamic interactions, nanosuspensions were subject to both hydrodynamic and Brownian interactions.

Table 1. Details of coarse suspensions (22 sets).

Set No	Range of ϕ	Description	Source
1	0–0.50	Spherical particles of glass 100–160 μm in diameter.	Vand [21]
2–3	0–0.30	Spherical non-colloidal particles made from methyl methacrylate. The ratio of large to small diameters in set 2 was 1.6:1. For set 3, the ratio was 3:1.	Ward and Whitmore [22]
4	0–0.512	Spherical particles of glass of average diameter 230 μm .	Ting and Luebbers [33]
5	0–0.50	The data were extracted from the plot representing the average of the experimental viscosity data of many non-colloidal suspensions of spherical particles.	Rutgers [35]

Table 1. *Cont.*

Set No	Range of ϕ	Description	Source
6	0–0.57	The data were extracted from the plot representing the average of the experimental viscosity data of many non-colloidal suspensions of spherical particles.	Thomas [36]
7	0.50–0.576	Spherical monomodal particles of glass with diameters in the range of 53.8 to 236 μm .	Chong et al. [38]
8	0–0.40	Monomodal spherical particles ranging in diameter from 51.8 to 240.3 μm .	
9	0–0.397	Spherical particles of glass 5–10 μm in diameter.	Lewis and Nielsen [39]
10	0–0.410	Spherical particles of glass 30–40 μm in diameter.	
11	0–0.50	Spherical particles of glass 45–60 μm in diameter.	
12	0–0.45	Spherical particles of glass 90–105 μm in diameter.	
13–14	0–0.50	Spherical monodisperse particles of glass. For set 13, average diameter was 26 μm . For set 14, average diameter was 61 μm .	Smith [42]
15	0–0.5236	Spherical monodisperse particles of glass with mean diameter of 125 μm .	Smith [42]
16	0–0.55	Spherical monodisperse particles of glass with mean diameter of 183 μm .	
17	0–0.50	Spherical monodisperse particles of glass with mean diameter of 221 μm .	
18	0–0.398	Spherical particles of polystyrene with mean diameter of 700 μm .	Ilic and Phan-Thien [54]
19	0–0.50	Spherical particles of glass with mean diameter $43 \pm 5.7 \mu\text{m}$.	Zarraga et al. [58]
20	0.41–0.58	Poly (methyl methacrylate) particles, diameter of 1100 μm ; polystyrene particles, diameter of 580 μm .	Boyer et al. [74]
21	0–0.45	Spherical particles of polystyrene with mean diameter of 40 μm .	Tanner et al. [66]
22	0–0.60	Particles of limestone with average diameter 4.91 μm .	Wilms et al. [75]

Table 2. Details of nanosuspensions (16 sets).

Set No	Type and Diameter of Nanoparticles	Temp ($^{\circ}\text{C}$)	Reference
1–4	Oil nanodroplets: set 1 (27.5 nm), set 2 (58.5 nm), set 3 (102 nm), set 4 (205 nm)	20	Van der Waarden [30]
5	Silica: 156 nm	20	de Kruif et al. [76]
6–8	Silica: set 6 (56 nm), set 7 (96 nm), set 8 (245 nm)	20	Van der Werff and De Kruif [77]
9	Silica: 50 nm	20	Jones et al. [52]
10	Polymer: 56 nm	20	Jones et al. [53]
11–12	Polystyrene latex: set 11 (282 nm), set 12 (168 nm)	20	Rodriguez et al. [78]
13	Silica of three different sizes: 113, 280, and 427 nm	–10	Shikata and Pearson [79]
14	Polystyrene latex: 146 nm	20	Weiss et al. [56]
15	CuO: 29 nm	22–25	Nguyen et al. [80]
16	Al_2O_3 : 36 nm	22–25	Nguyen et al. [81]

Table 3. Details of the SNP-thickened coarse suspensions (6 sets).

Set No	SNP Concentration of Matrix Phase (wt%)	Type and Size of Solid Particles	Concentration Range of Solid Particles (vol%)	Reference
1–6	Set 1 (9.89%), set 2 (14.83%), set 3 (19.75%), set 4 (24.71%), set 5 (29.67%), set 6 (34.60%)	Ceramic hollow spheres, 10 to 340 μm ; Sauter mean diameter of 138 μm	Set 1 (0–55.08%), set 2 (0–54.54%), set 3 (0–56%), set 4 (0–53.44%), set 5 (0–51.93%), set 6 (0–50.36%)	Ghanaatpishehsanaei and Pal [82]

The relative viscosity versus particle volume fraction data for the coarse suspensions (22 sets) are shown in Figure 4. The data for all the suspensions in this group tend to fall on the same curve. The relative viscosity versus particle volume fraction data for the sixteen sets of nanosuspensions, as shown in Figure 5, also fall on the same curve. The six sets of data for the coarse suspensions thickened by starch nanoparticles (SNPs), as shown in Figure 6, generally tend to fall on the same curve, regardless of the SNP concentration of the matrix phase. However, some scattering of data can be observed for low-volume fractions of solid particles.

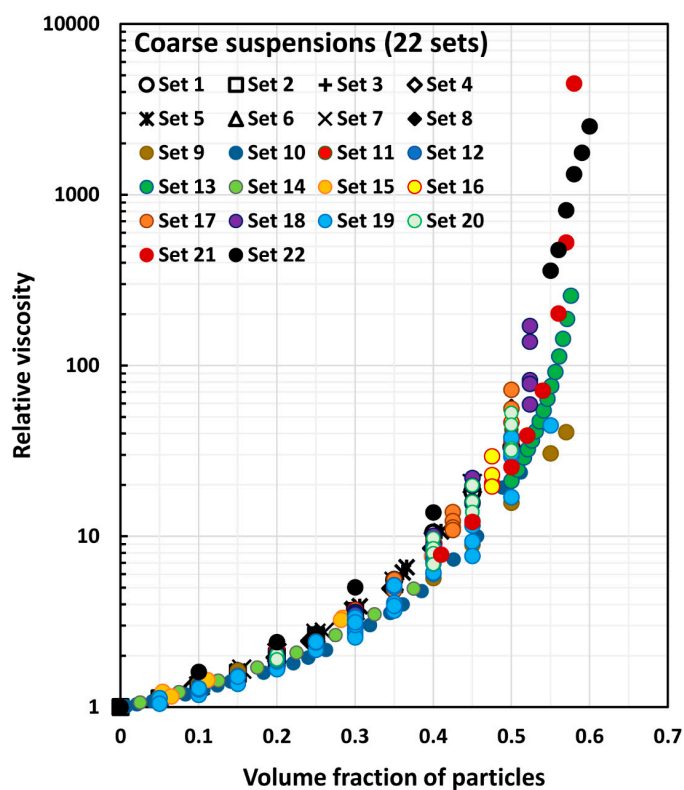
**Figure 4.** Experimental relative viscosity versus particle volume fraction data for twenty-two sets of coarse suspensions.

Figure 7 shows all the experimental data (44 sets) together for coarse suspensions, nanosuspensions, and SNP-thickened coarse suspensions. The data for different groups of suspensions do not seem to overlap with each other. The reason for this observation is that the packing structure, and, hence, the maximum packing volume fraction, of suspensions is not the same for these different groups of suspensions.

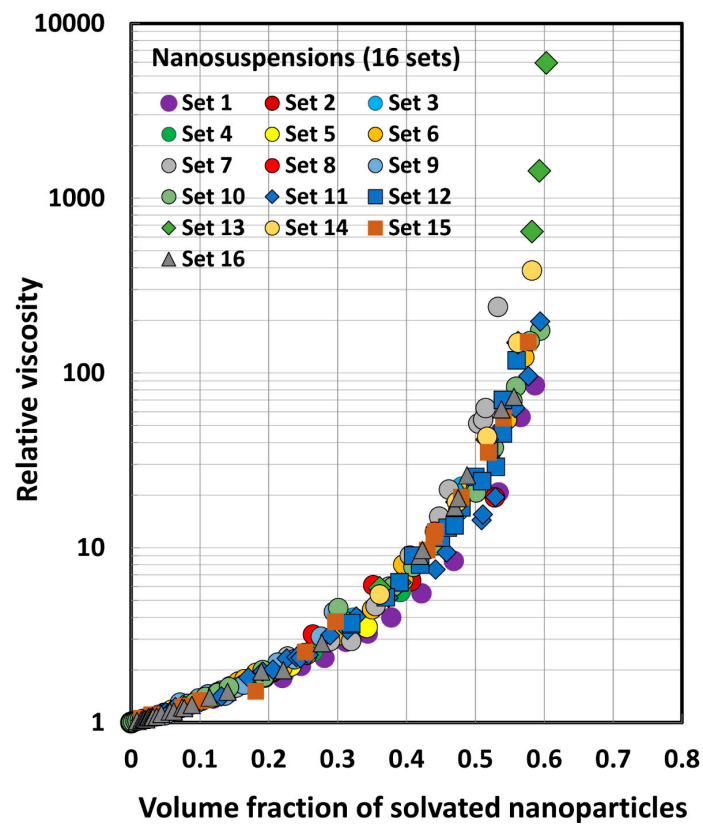


Figure 5. Experimental relative viscosity versus particle volume fraction data for sixteen sets of nanosuspensions.

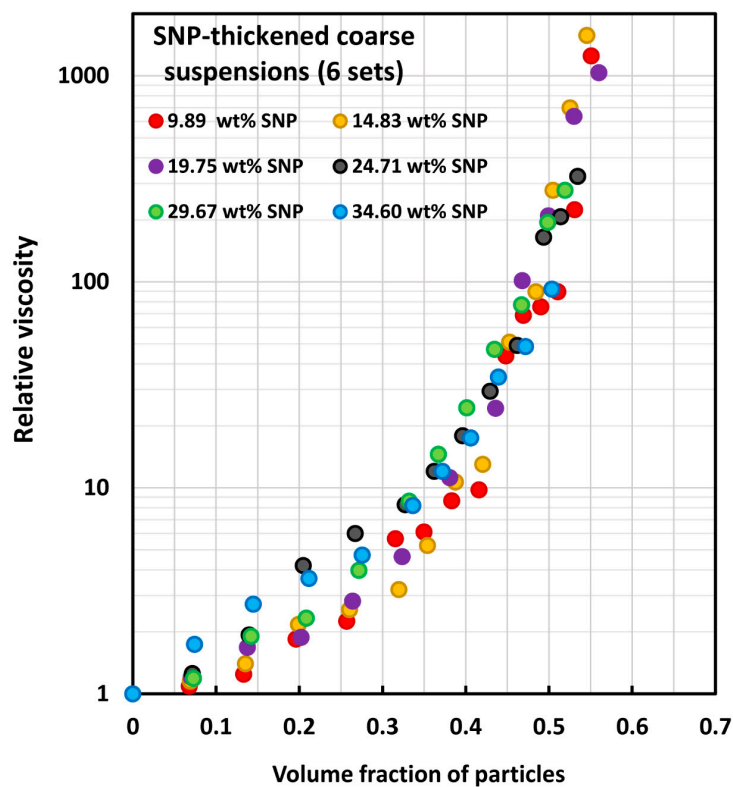


Figure 6. Experimental relative viscosity versus particle volume fraction data for six sets of SNP-thickened coarse suspensions.

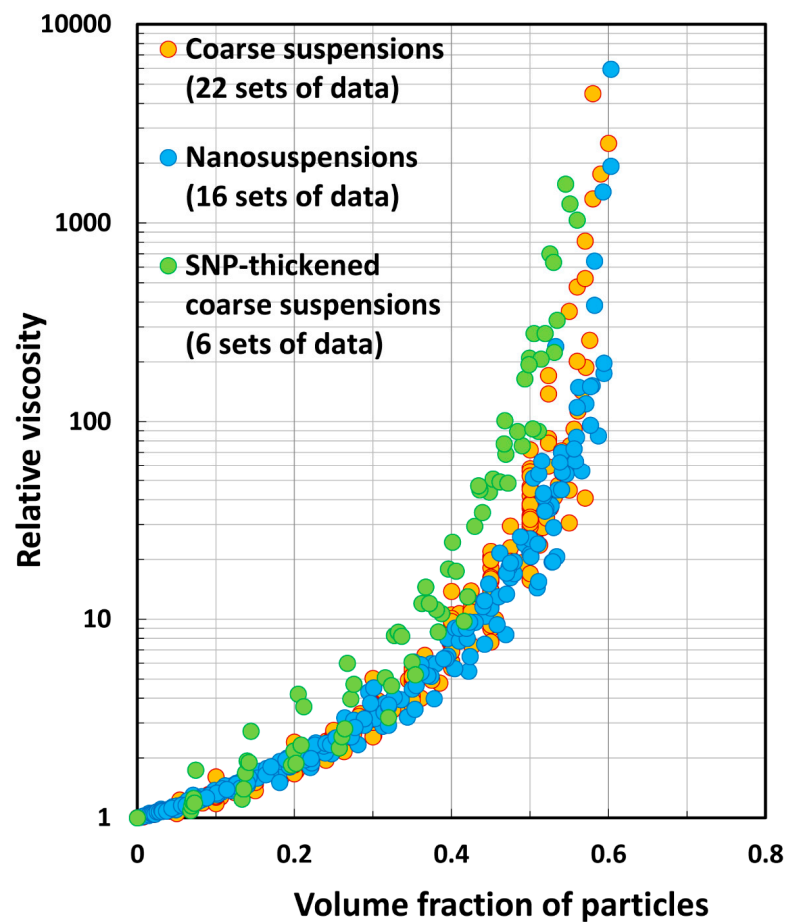


Figure 7. Experimental relative viscosity versus particle volume fraction data for all the suspensions (44 sets), including coarse suspensions, nanosuspensions, and SNP-thickened coarse suspensions.

5.2. Estimation of Maximum Packing Volume Fraction of Suspensions

The maximum packing volume fraction of suspensions is estimated from the relative viscosity versus particle concentration data at high particle concentrations ($\phi > 0.3$). A linear relationship can be observed when the data are plotted as $\eta_r^{-0.4}$ versus ϕ . This linear relationship can be extended to $\eta_r^{-0.4} = 0$ to estimate ϕ_m . A similar approach was used by Tanner [83] to estimate ϕ_m for suspensions.

Figures 8–10 show the plots of $\eta_r^{-0.4}$ versus ϕ for the three group of suspensions: coarse suspensions (Figure 8), nanosuspensions (Figure 9), and SNP-thickened coarse suspensions (Figure 10). The estimated values of ϕ_m are as follows: coarse suspensions, $\phi_m = 0.632$; nanosuspensions, $\phi_m = 0.652$; SNP-thickened coarse suspensions, $\phi_m = 0.57$. Note that the maximum packing volume fraction is 0.637 for random close packing of hard spheres. The packing volume fraction of particles is 0.58 at glass transition of hard spheres. Thus, the ϕ_m values for the coarse suspensions and nanosuspensions are close to the random packing of hard spheres, whereas the ϕ_m value for SNP-thickened coarse suspensions is almost equal to the glass transition volume fraction of hard spheres corresponding to $\phi_m = 0.58$.

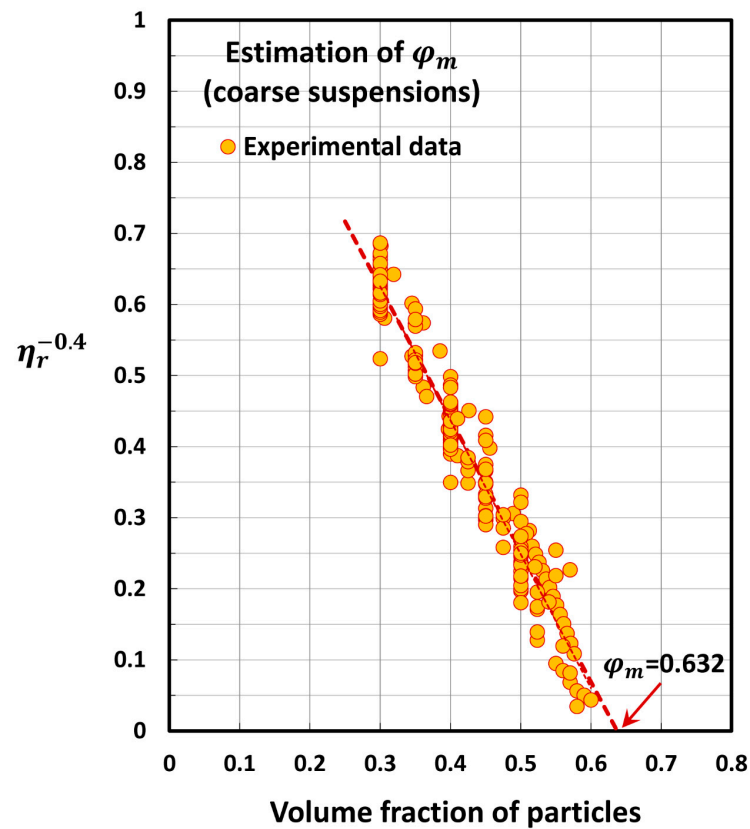


Figure 8. Estimation of the maximum packing volume fraction for coarse suspensions.

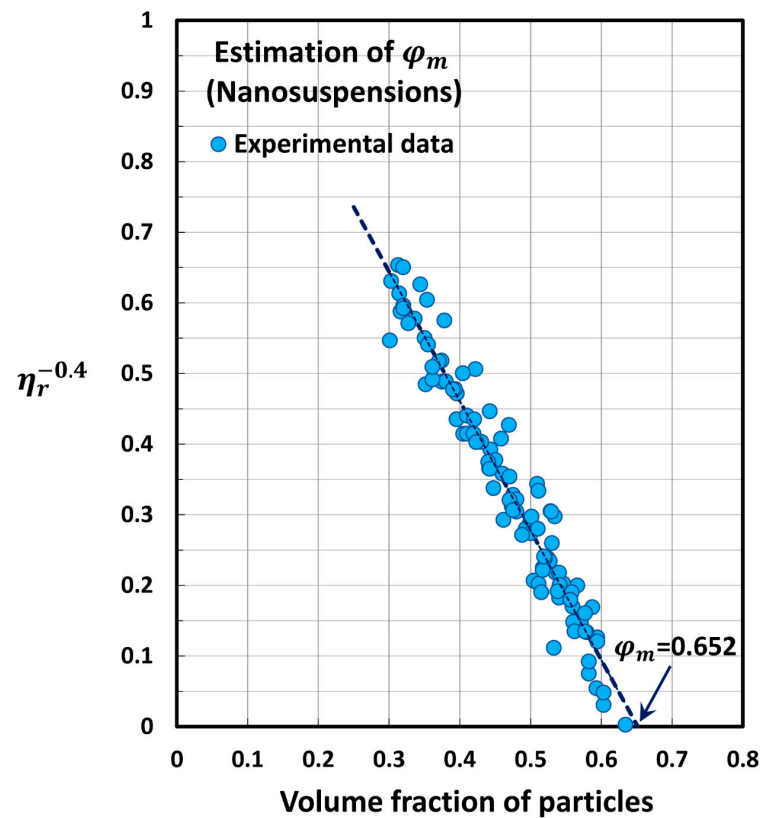


Figure 9. Estimation of the maximum packing volume fraction for nanosuspensions.

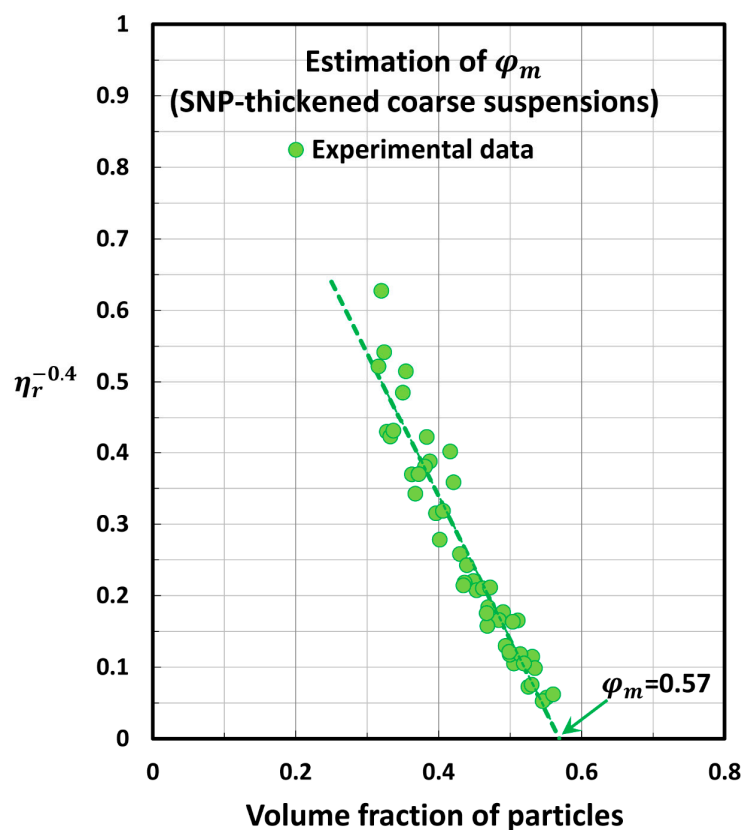


Figure 10. Estimation of the maximum packing volume fraction for SNP-thickened coarse suspensions.

5.3. Model Predictions Versus Experimental Data

Figures 11–18 compare the predictions of the viscosity models (eight models) with the experimental data. Figure 11 compares the predictions of the Mooney model with the three groups of experimental data (coarse suspensions, nanosuspensions, and SNP-thickened coarse suspensions). The φ_m values estimated in the preceding section are used in the model. Likewise, Krieger–Dougherty model comparisons are shown in Figure 12, Cheng et al. model comparisons are shown in Figure 13, Mendoza and Santamaria-Holek model comparisons are shown in Figure 14, Brouwers model comparisons are shown in Figure 15, Pal model P1 comparisons are shown in Figure 16, Pal model P2 comparisons are shown in Figure 17, and Pal model P3 comparisons are shown in Figure 18.

The comparisons of the model predictions with the experimental data shown in Figures 11–18 reveal the following information:

- The Mooney model (M) overpredicts the relative viscosity of suspensions.
- The Krieger–Dougherty model (KD) underpredicts the relative viscosity of suspensions.
- The Cheng et al. model (C) overpredicts the relative viscosity at low and high particle concentrations.
- The Mendoza and Santamaria-Holek model (MS) underpredicts the relative viscosity of suspensions.
- The Brouwers model (B) overpredicts the relative viscosity of suspensions.
- Pal model P1 overpredicts the relative viscosity of suspensions.
- Pal model P2 underpredicts the relative viscosity of suspensions.
- Pal model P3 predictions are close to experimental values.

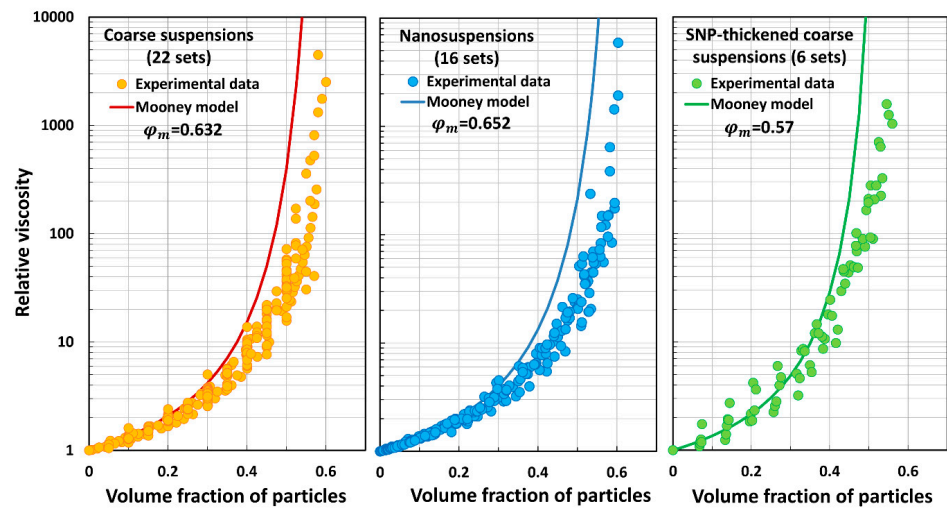


Figure 11. Comparisons of Mooney model predictions with experimental data.

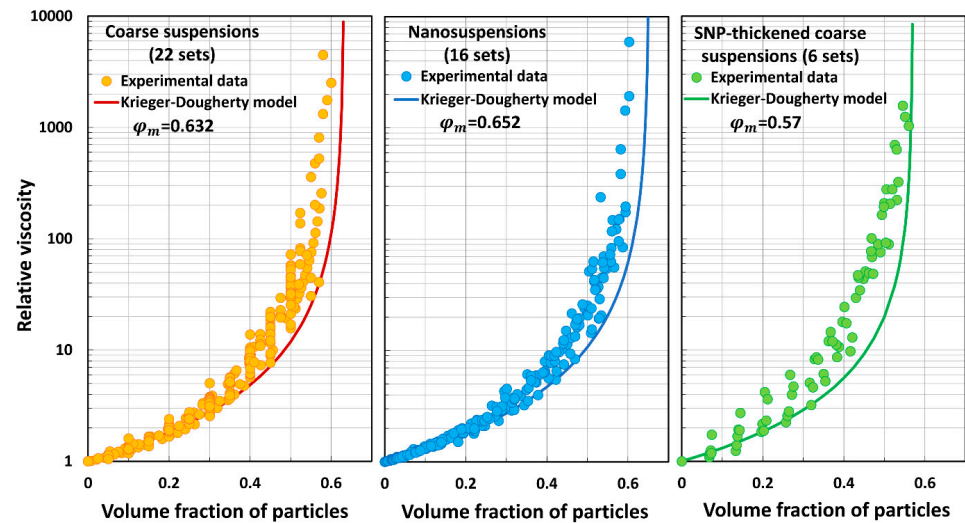


Figure 12. Comparisons of Krieger–Dougherty model predictions with experimental data.

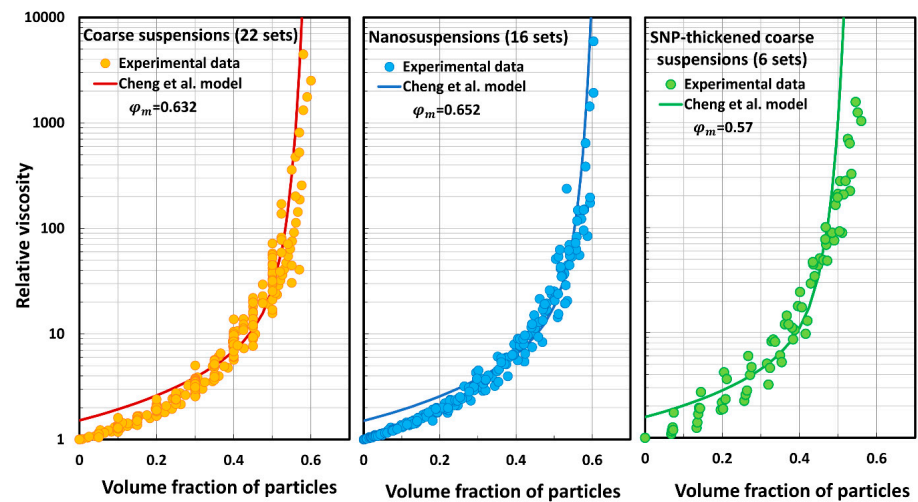


Figure 13. Comparisons of Cheng et al. model predictions with experimental data.

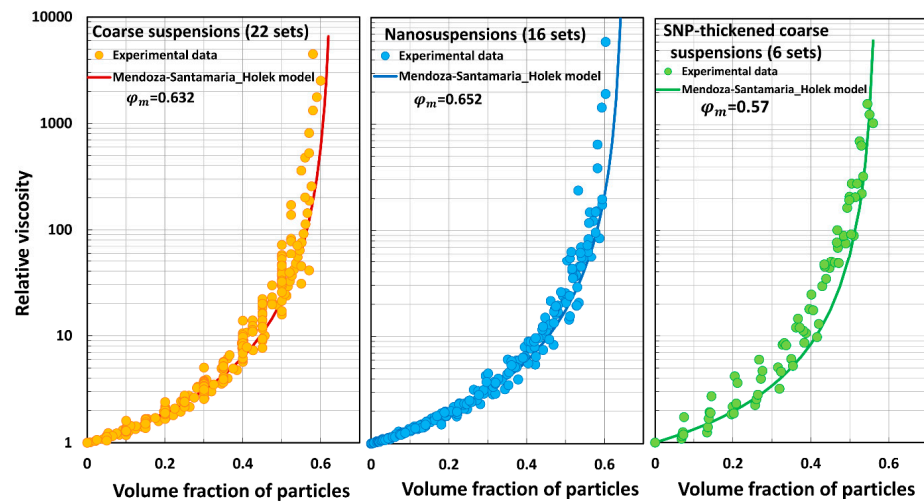


Figure 14. Comparisons of Mendoza and Santamaria-Holek model predictions with experimental data.

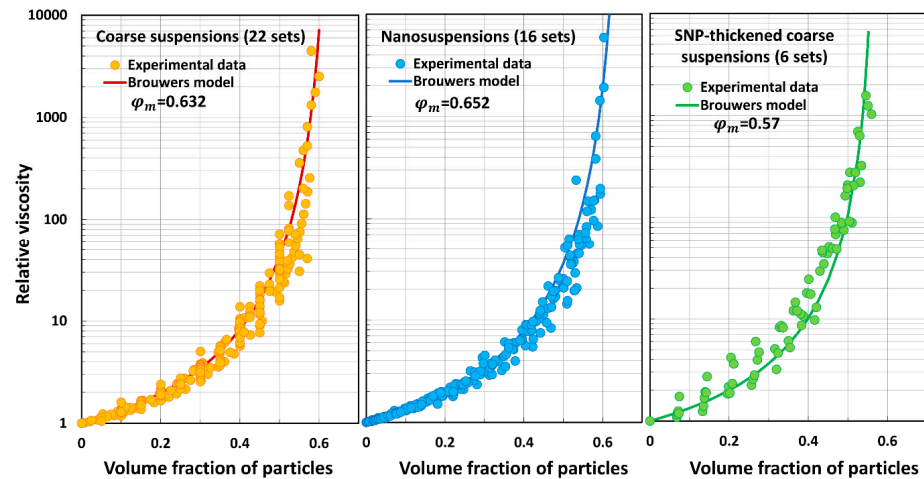


Figure 15. Comparisons of Brouwers model predictions with experimental data.

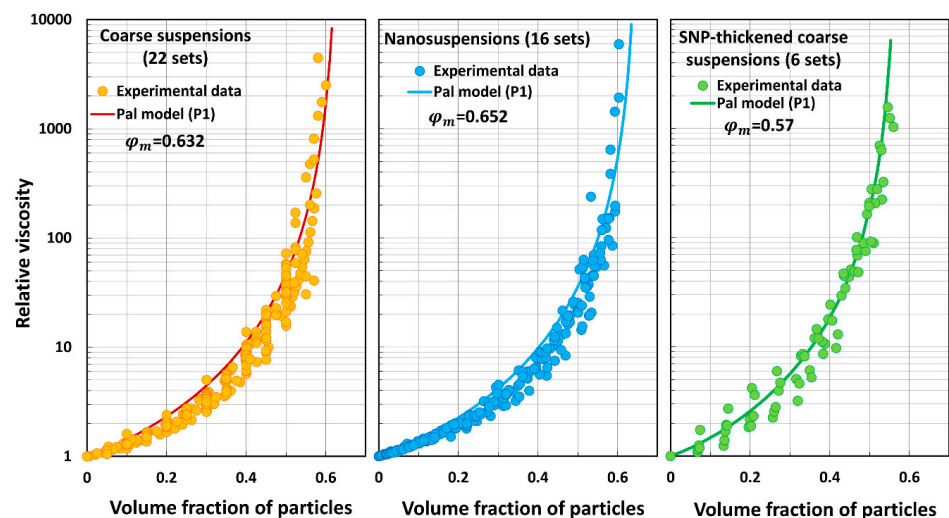


Figure 16. Comparisons of Pal model P1 predictions with experimental data.

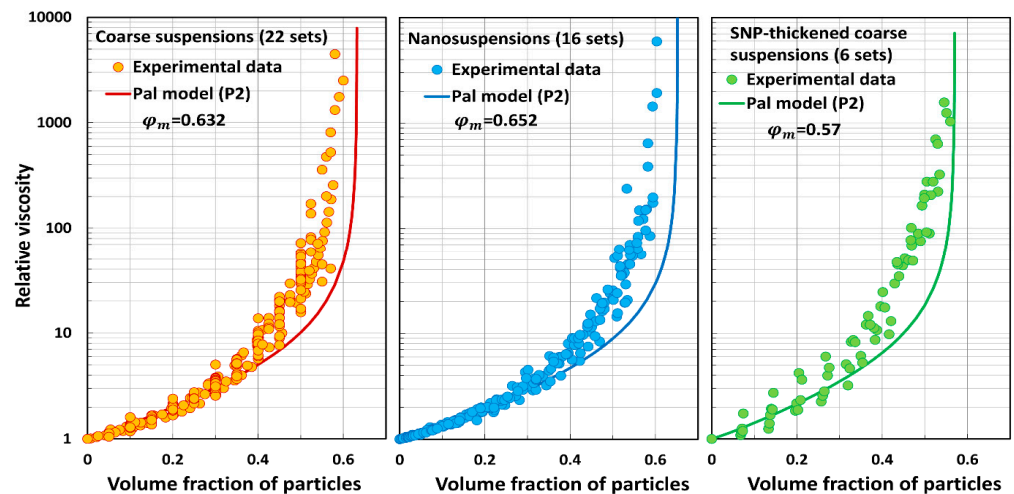


Figure 17. Comparisons of Pal model P2 predictions with experimental data.

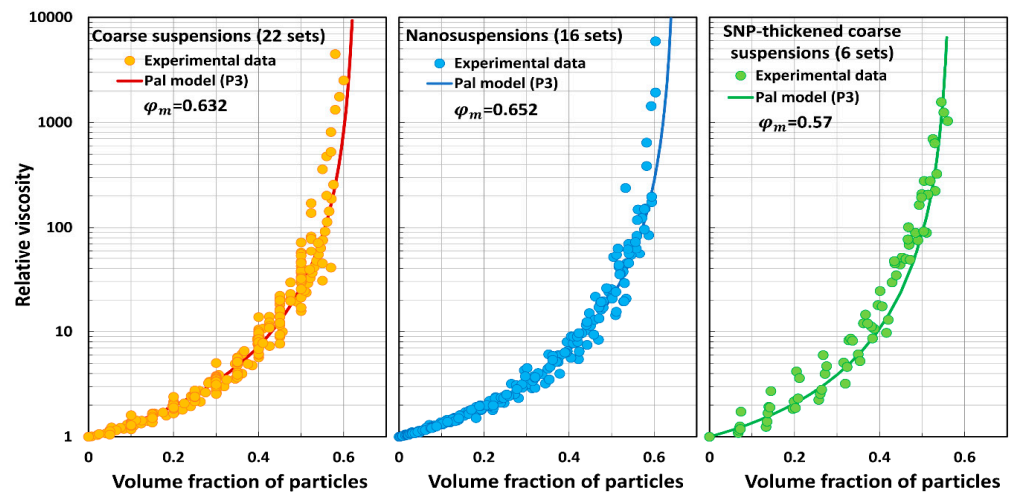


Figure 18. Comparisons of Pal model P3 predictions with experimental data.

Table 4 summarizes the average percentage relative error (APRE) values calculated for each model. The APRE is defined as follows:

$$APRE = \frac{1}{n} \sum_{i=1}^{i=n} \frac{(\eta_{r,exp})_i - (\eta_{r,mod})_i}{(\eta_{r,exp})_i} \times 100 \quad (47)$$

where the subscripts “*exp*” and “*mod*” refer to experimental value and model predicted value, and *n* is the number of data points. Based on the average percent error, the deviations of model predictions are grouped into five categories as indicated below:

- Magnitude of APRE $\leq 5\%$: deviation in model prediction: Slight;
- $5\% < \text{Magnitude of APRE} \leq 10\%$: deviation in model prediction: Moderate;
- $10\% < \text{Magnitude of APRE} \leq 30\%$: deviation in model prediction: Substantial;
- $30\% < \text{Magnitude of APRE} \leq 100\%$: deviation in model prediction: Severe;
- Magnitude of APRE $> 100\%$: deviation in model prediction: Extreme.

Table 4. APRE values for different models.

Model Type	Coarse Suspensions	Nanosuspensions	SNP-Thickened Coarse Suspensions
Mooney model (M)	$-8.98 \times 10^8\%$ (Overpredicts extremely)	$-1.64 \times 10^{18}\%$ (Overpredicts extremely)	$-3.88 \times 10^{31}\%$ (Overpredicts extremely)
Krieger–Dougherty model (KD)	27.55% (Underpredicts substantially)	23.05% (Underpredicts substantially)	47.73% (Underpredicts severely)
Cheng et al. model (C)	-3531% (Overpredicts extremely)	$-1.14 \times 10^7\%$ (Overpredicts extremely)	$-2.16 \times 10^{22}\%$ (Overpredicts extremely)
Mendoza and Santamaria-Holek model (MS)	12.56% (Underpredicts substantially)	10.43% (Underpredicts substantially)	23.96% (Underpredicts substantially)
Brouwers model (B)	-21.6% (Overpredicts substantially)	-32.43% (Overpredicts severely)	-43.4% (Overpredicts severely)
Pal model one (P1)	-34.81% (Overpredicts severely)	-26.01% (Overpredicts severely)	-56.42% (Overpredicts severely)
Pal model two (P2)	24.85% (Underpredicts substantially)	22.96% (Underpredicts substantially)	42.64% (Underpredicts severely)
Pal model three (P3)	3.22% (Underpredicts slightly)	3.51% (Underpredicts slightly)	6.37% (Underpredicts moderately)

The Mooney and Cheng et al. models overpredict the relative viscosity values of coarse suspensions, nanosuspensions, and SNP-thickened coarse suspensions in an extreme way. The average percentage error is very large (>3531). These models are clearly not suitable for the prediction of the relative viscosities of suspensions. The Krieger–Dougherty model underpredicts the relative viscosities of suspensions substantially to severely. The Mendoza and Santamaria-Holek model underpredicts the relative viscosities substantially. The Brouwers model overpredicts the relative viscosities substantially to severely. Pal model P1 overpredicts the relative viscosities severely. Pal model P2 underpredicts the relative viscosities substantially to severely. Pal model P3 is the best model in that it deviates from the experimental data only slightly to moderately.

As Pal model P3 shows relatively small deviations from the experimental data, a master curve for the relative viscosity of coarse suspensions, nanosuspensions, and SNP-thickened coarse suspensions was developed based on this model. Figure 19 shows the master curve based on Pal model P3. The data are plotted as relative viscosity versus effective volume fraction of particles (φ_{eff}), where φ_{eff} is given by Equation (45). The experimental data for all the suspensions fall on the master curve generated by Pal model P3. Some scatter in the experimental data observed around the master curve could probably be explained in terms of friction between the particles of the suspensions. We have assumed that the suspension particles are smooth with negligible friction. Several recent studies [83,84] have indicated that the role of friction between particles is important in determining the viscosity of suspensions.

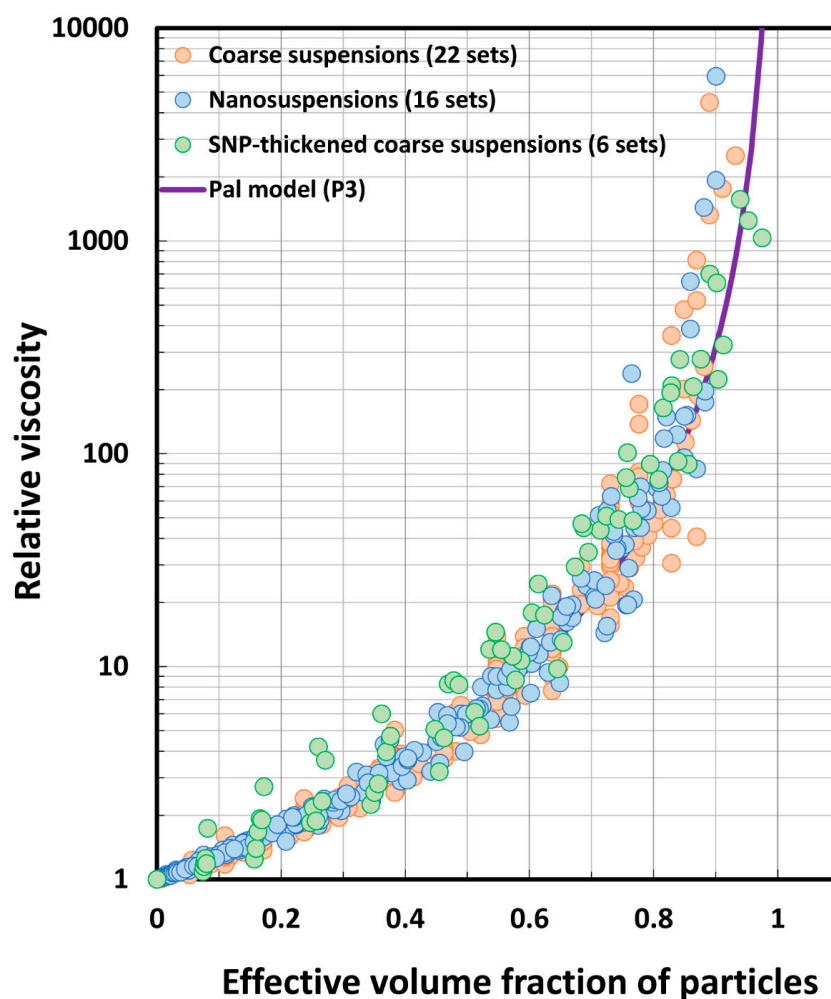


Figure 19. Master curve generated by Pal model P3 (Equation (46)). The experimental data for all the suspensions (coarse suspensions, nanosuspensions, and SNP-thickened coarse suspensions) overlap with each other, which is in agreement with Pal model P3.

6. Simulation of the Viscous Behavior of Concentrated Multimodal Suspensions

From a practical point of view, it is important to formulate suspensions with as high a concentration of particles as possible while keeping the viscosity reasonable. As can be observed in the preceding sections, the viscosity of unimodal suspensions becomes infinite when the particle concentration, φ , reaches the maximum packing volume fraction, φ_m . For random packing of uniform hard spheres, the value of φ_m is 0.637. Thus, it is impossible to load a suspension with particles above a particle concentration (volume fraction) of 0.637. Interestingly, the loading of suspensions with particles exceeding a concentration of 0.637 can be readily achieved by making the suspension multimodal while keeping the viscosity of the suspension reasonable at the same time. Alternatively, the viscosity of the suspension can be reduced substantially at a fixed particle concentration by making the suspension multimodal.

Consider the formulation of a multimodal suspension consisting of N different-size particles. Let V_L be the volume of the initial suspending medium liquid (matrix phase without any particles). Let $V_1, V_2, V_3, \dots, V_n, V_{n+1}, \dots, V_N$ be the volumes of different-size particles added successively to the initial liquid of volume V_L . We assume that each new set of particles added is much larger in size than the previous set of particles. Thus, V_1 is

the volume of smallest-size particles in the suspension, and V_N is the volume of largest-size particles. Let the apparent concentrations of different-size particles be defined as follows:

$$\varphi_1 = \frac{V_1}{V_L + V_1}, \varphi_2 = \frac{V_2}{V_L + V_1 + V_2}, \varphi_3 = \frac{V_3}{V_L + V_1 + V_2 + V_3} \quad (48)$$

$$\varphi_n = \frac{V_n}{(V_L + V_1 + V_2 \cdots + V_{n-1}) + V_n} = \frac{V_n}{V_L + \sum_{i=1}^n V_i} \quad (49)$$

where φ_n is the apparent concentration of any n th set of particles, and n could be any number from 1 to N . Note that φ_n is not the actual concentration (volume fraction) of the n th set of particles. The actual concentration of any n th set of particles is given as follows:

$$\varphi_{n, \text{actual}} = \frac{V_n}{V_L + \sum_{i=1}^N V_i} \quad (50)$$

The denominator on the right-hand side of Equation (50) is the total volume of the suspension.

The actual total concentration of particles (φ_T) is given as follows:

$$\varphi_T = \frac{\sum_{i=1}^N V_i}{V_L + \sum_{i=1}^N V_i} \quad (51)$$

It can be readily shown that [85]:

$$1 - \varphi_T = \prod_{i=1}^N (1 - \varphi_i) \quad (52)$$

where \prod is the product sign.

Now consider two successive stages, (i) and ($i + 1$), in the process of the addition of different-size particles to formulate a multimodal suspension of N particle sizes. Following the effective medium approach, the suspension of stage (i) can be treated as an effective medium that is homogeneous with respect to the new set of particles added to reach stage ($i + 1$). For the effective medium approach to be valid, it is assumed that the new set of particles added at stage ($i + 1$) is much larger (ten times) than the set of particles added in the previous stage (i). Consequently, the relative viscosity of the multimodal suspension can be expressed as follows:

$$\eta_r = \prod_{i=1}^N H(\varphi_i) \quad (53)$$

where H is the relative viscosity function of a suspension. We use Pal model P3 (Equation (46)) for the relative viscosity function:

$$H(\varphi_i) = \left[1 - \left\{ 1 + \left(\frac{1 - \varphi_m}{\varphi_m^2} \right) \varphi_i \right\} \varphi_i \right]^{-2.5} \quad (54)$$

where φ_m is taken to be 0.637, corresponding to random close packing of hard spheres. From Equations (53) and (54), it follows that:

$$\eta_r = \prod_{i=1}^N \left[1 - \left\{ 1 + \left(\frac{1 - \varphi_m}{\varphi_m^2} \right) \varphi_i \right\} \varphi_i \right]^{-2.5} \quad (55)$$

Equation (55) can be used to predict the relative viscosity of multimodal suspensions.

6.1. Relative Viscosity of Bimodal Suspensions

For bimodal suspensions, Equation (55) simplifies to the following:

$$\eta_r = \left[1 - \left\{ 1 + \left(\frac{1 - \varphi_m}{\varphi_m^2} \right) \varphi_1 \right\} \varphi_1 \right]^{-2.5} \left[1 - \left\{ 1 + \left(\frac{1 - \varphi_m}{\varphi_m^2} \right) \varphi_2 \right\} \varphi_2 \right]^{-2.5} \quad (56)$$

Given the total concentration of particles, φ_T , and fraction of coarse particles in the mixture of fine and coarse particles, we can estimate the relative viscosity of bimodal suspensions from Equation (56). If the fraction of coarse particles in the mixture of fine and coarse particles is f_c , it can be readily shown that:

$$\varphi_2 = f_c \varphi_T \quad (57)$$

$$\varphi_1 = \frac{\varphi_T - \varphi_2}{1 - \varphi_2} \quad (58)$$

Equation (58) follows from the simplification of Equation (52) for a bimodal system.

Figure 20 shows the relative viscosities of bimodal suspensions calculated from Equations (56)–(58) for different values of total particle concentration, φ_T . As already noted, we used $\varphi_m = 0.637$ in the calculations. Interestingly, the relative viscosity of a suspension decreases substantially by changing a monomodal suspension to a bimodal suspension while keeping the total particle concentration, φ_T , constant. The effect of the bimodality of suspension on the relative viscosity is especially strong at high values of φ_T . As an example, the relative viscosity of a unimodal suspension at a total particle concentration, φ_T , of 0.63 is 36,696. A sharp reduction in the relative viscosity of suspension from 36,696 to 43 can be observed when the single-size (uniform) particles of a unimodal suspension are replaced by a mixture of large and small particles with a large particle fraction of 0.60. Note that the relative viscosity of the suspension is minimum (see Figure 20) at a coarse particle fraction of 0.60 when $\varphi_T = 0.63$.

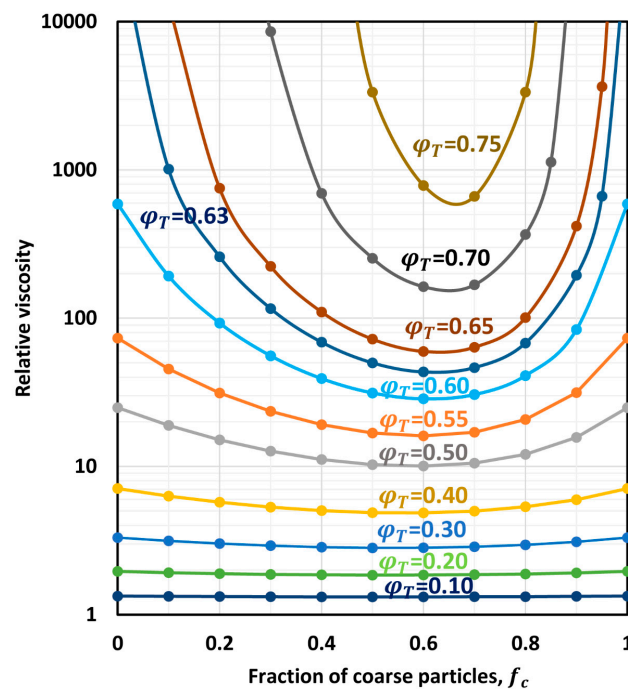


Figure 20. Relative viscosity of bimodal suspensions as a function of coarse particle fraction of the particle mixture.

6.2. Minimum Relative Viscosity of Multimodal Suspensions

Figure 20 reveals that the relative viscosity of a bimodal suspension at a fixed φ_T becomes minimum at a certain fraction of coarse particles in a mixture of fine and coarse particles. This observation is not restricted to bimodal suspensions. It is true for any multimodal suspension.

Farris [85] has shown that a minimum in the relative viscosity of a multimodal suspension occurs when:

$$\varphi_1 = \varphi_2 = \varphi_3 = \dots = \varphi_N = \varphi_o \quad (59)$$

Equation (59) indicates that the minimum in the relative viscosity of multimodal suspensions occurs when the apparent concentrations, φ_i , of all particle sizes are equal. The apparent concentrations of different particle-size fractions are defined in Equations (48) and (49). The common value of φ_i , denoted as φ_o , where minimum relative viscosity occurs can be calculated from Equation (52) as follows:

$$1 - \varphi_T = (1 - \varphi_o)^N \quad (60)$$

$$\varphi_o = 1 - (1 - \varphi_T)^{1/N} \quad (61)$$

Thus, the minimum viscosity of a multimodal suspension can be calculated from Equation (55) as follows:

$$\eta_r = \left[1 - \left\{ 1 + \left(\frac{1 - \varphi_m}{\varphi_m^2} \right) \varphi_o \right\} \varphi_o \right]^{-2.5N} \quad (62)$$

Figure 21 shows the plots of relative viscosity of different multimodal suspensions (unimodal, bimodal, trimodal, octamodal, and decamodal) as a function of total particle concentration, φ_T . The plots are generated from Equation (62); therefore, they represent the minimum relative viscosity plots for different multimodal suspensions. Interestingly, a large drop in relative viscosity can be observed when the modality of the suspension is increased at any given φ_T . However, the decrease in relative viscosity reaches a limit. The limiting relative viscosity plot corresponding to an infinitely multimodal suspension is given by the following Roscoe–Brinkman equation:

$$\eta_r = (1 - \varphi)^{-2.5}$$

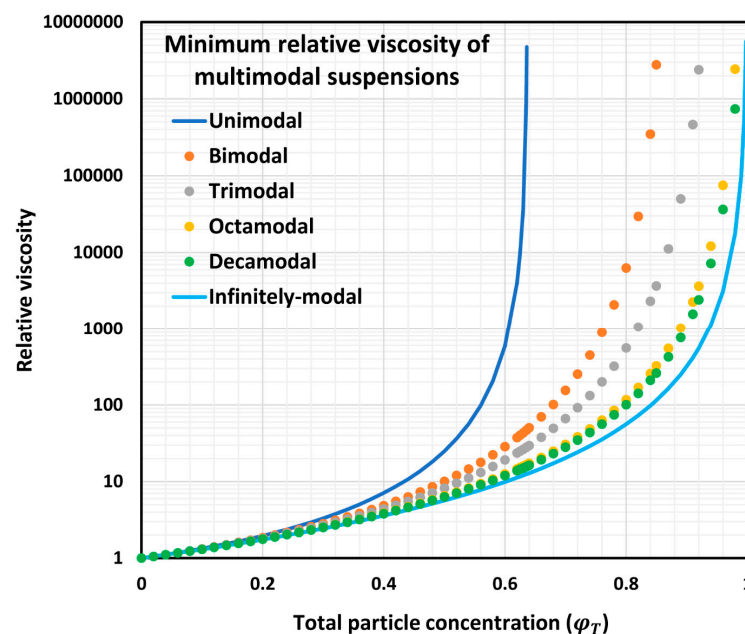


Figure 21. Minimum relative viscosity of multimodal suspensions as a function of total particle concentration, φ_T .

This equation was originally derived by Roscoe [25] and Brinkman [26] independently to describe the relative viscosities of an infinitely multimodal suspension. Note that φ in this equation is the total particle concentration, φ_T .

6.3. Composition of Multimodal Suspensions at Minimum Relative Viscosity

Equation (62) allows the calculation of the minimum relative viscosity at a given φ_T for a multimodal suspension of any modality N . However, it does not give the composition of the multimodal suspension. For example, consider a trimodal suspension consisting of three different particle-size fractions: coarse, medium, and fine particles. For an engineer to formulate this trimodal suspension with a minimum viscosity at a given φ_T , it is important to know the composition in terms of the fractions of coarse, medium, and fine particles in the total mixture of particles.

The calculation of the composition of a suspension is complicated. We will consider only a trimodal suspension and develop equations to calculate the composition where the relative viscosity is minimum. A similar approach can be used for any other multimodal suspension. Let the total particle concentration be φ_T , the fraction of coarse particles in the particle mixture be f_c , the fraction of medium-size particles be f_m , and the fraction of fine particles be f_f . From Equation (48), we can express the volumes of different fractions of particles as follows:

$$V_1 = \left(\frac{\varphi_1}{1-\varphi_1}\right)V_L, V_2 = \left(\frac{\varphi_2}{1-\varphi_2}\right)\left(\frac{1}{1-\varphi_1}\right)V_L, V_3 = \left(\frac{\varphi_3}{1-\varphi_3}\right)\left[1 + \left(\frac{\varphi_1}{1-\varphi_1}\right) + \frac{\varphi_2}{(1-\varphi_1)(1-\varphi_2)}\right]V_L \quad (63)$$

The fractions of different particle sizes in the mixture of particles are as follows:

$$f_c = \frac{V_3}{V_1 + V_2 + V_3}, f_m = \frac{V_2}{V_1 + V_2 + V_3}, f_f = 1 - f_c - f_m \quad (64)$$

By definition,

$$\varphi_T = \frac{V_1 + V_2 + V_3}{V_L + V_1 + V_2 + V_3}, \varphi_3 = \frac{V_3}{V_L + V_1 + V_2 + V_3} \quad (65)$$

Thus, the fraction of coarse particles can be expressed as follows:

$$f_c = \frac{V_3}{V_1 + V_2 + V_3} = \frac{\varphi_3}{\varphi_T} \quad (66)$$

Using Equation (63), the fraction of medium-size particles in the particle mixture can be expressed as follows:

$$f_m = \frac{V_2}{V_1 + V_2 + V_3} = \frac{\varphi_2 / [(1-\varphi_1)(1-\varphi_2)]}{\left(\frac{\varphi_1}{1-\varphi_1}\right) + \left(\frac{\varphi_2}{1-\varphi_2}\right)\left(\frac{1}{1-\varphi_1}\right) + \left(\frac{\varphi_3}{1-\varphi_3}\right)\left[1 + \left(\frac{\varphi_1}{1-\varphi_1}\right) + \frac{\varphi_2}{(1-\varphi_1)(1-\varphi_2)}\right]} \quad (67)$$

As $\varphi_1 = \varphi_2 = \varphi_3 = \varphi_o$ at the minimum relative viscosity, the fractions f_c , f_m , and f_f can be expressed in terms of the known values of φ_o (Equation (61)) and φ_T as follows:

$$f_c = \frac{\varphi_o}{\varphi_T}, f_m = \frac{1-\varphi_o}{1+(1-\varphi_o)(2-\varphi_o)}, f_f = 1 - f_c - f_m \quad (68)$$

Table 5 summarizes the calculations for trimodal suspensions giving minimum relative viscosities and the corresponding compositions for different values of total particle concentration.

Table 5. Minimum relative viscosity and corresponding composition of trimodal suspensions.

φ_T	φ_O	η_r	f_c	f_m	f_f
0.50	0.21	8.18	0.41	0.33	0.26
0.55	0.23	12.07	0.42	0.33	0.25
0.60	0.26	19.10	0.44	0.32	0.24
0.65	0.30	33.26	0.45	0.32	0.23
0.70	0.33	66.28	0.47	0.32	0.21
0.75	0.37	161.98	0.49	0.31	0.20
0.80	0.42	555.34	0.52	0.30	0.18
0.85	0.47	3662.97	0.55	0.29	0.16
0.89	0.52	49,779.29	0.59	0.28	0.13

7. Conclusions

The relative viscosity models for suspensions of hard spheres proposed in the 21st century, along with the classical models of Mooney and Krieger–Dougherty, published in the 1950s, were reviewed, compared, and evaluated using a large pool of experimental data available on coarse suspensions, nanosuspensions, and coarse suspensions thickened by starch nanoparticles. The Mooney model (Equation (13)) gives the worst performance in that the magnitude of the average percentage error is extremely large ($APRE > 10^8$), the Cheng et al. model (Equation (16)) is the second worst performer with $APRE > 3531$, the Krieger–Dougherty model (Equation (15)) underpredicts the relative viscosities of suspensions substantially to severely ($23\% < APRE < 48\%$), the Mendoza and Santamaria-Holek model (Equation (23)) underpredicts the relative viscosities substantially ($10\% < APRE < 25\%$), the Brouwers model (Equation (26)) overpredicts the relative viscosities substantially to severely ($21\% < APRE < 44\%$), Pal model P1 (Equation (35)) overpredicts the relative viscosities severely ($26\% < APRE < 57\%$), and Pal model P2 (Equation (41)) underpredicts the relative viscosities substantially to severely ($23\% < APRE < 43\%$).

Clearly, the best available model in terms of the predictability of the relative viscosity of suspensions is Pal model P3 (Equation (46)). It gives reasonably good predictions of relative viscosities. The average percentage error for this model is in the range of 3 to 6.5 ($3\% < APRE < 6.5\%$).

Finally, the viscous behavior of multimodal suspensions was simulated using the Pal model P3 of unimodal suspensions. The influence of increasing the modality of particle sizes on the viscosity of suspensions was discussed, and the relationships for the minimum viscosity and the corresponding compositions for multimodal suspensions were developed.

Funding: This research was funded by the Discovery Grant awarded to R.P. by the Natural Sciences and Engineering Research Council of Canada.

Data Availability Statement: The data presented in this study are available on request from the author.

Conflicts of Interest: The author declares no conflict of interest.

Nomenclature

Greek Symbols

$\bar{\delta}$	Unit tensor
η	Viscosity
η_m	Viscosity of matrix phase (suspending medium)
η_r	Relative viscosity
$\eta_{r\infty}$	High-frequency relative viscosity
$\eta_{r,exp}$	Experimental value of relative viscosity
$\eta_{r,mod}$	Relative viscosity predicted by the model
$\Delta\eta_o$	Non-hydrodynamic contribution to relative viscosity (see Equation (16))
$\bar{\sigma}$	Bulk stress tensor
φ	Volume fraction of particles
φ_{eff}	Effective volume fraction of particles
φ_i	Volume fraction of i th set of particles in a multimodal suspension, defined in Equations (48) and (49)
φ_m	Maximum packing volume fraction of particles where the viscosity of suspension diverges
φ_n	Volume fraction of n th set of particles in a multimodal suspension, defined in Equations (48) and (49)
φ_o	Volume fraction of different-size particles in a multimodal suspension corresponding to minimum relative viscosity of suspension (see Equation (61))
φ_T	Total volume fraction of particles in a multimodal suspension, defined in Equation (51)
Ω	Self-crowding parameter, defined in Equation (28)

Latin Symbols

a	Constant in Equation (42)
APRE	Average percentage relative error
b	Constant in Equation (42)
c	Self-crowding parameter (see Equation (22))
\bar{E}	Bulk rate of strain tensor
\bar{E}_∞	Rate of strain tensor far away from the particle
f_c	Fraction (volume basis) of coarse particles in a bimodal or trimodal mixture of particles
f_f	Fraction (volume basis) of fine particles in a bimodal or trimodal mixture of particles
f_m	Fraction (volume basis) of medium-sized particles in a trimodal mixture of particles
GT	Glass transition point
H	Relative viscosity function
k	Aggregation coefficient (see Equation (42))
n	Number of data points or n th set of particles in a multimodal suspension
N	Number of different-size particle fractions in a multimodal suspension, same as modality
P	Pressure
R	Radius of particle
RCP	Random close packing
\bar{S}^0	Dipole strength of a single particle in an infinite matrix
V_1	Volume of smallest-size particles in a multimodal suspension
V_i	Volume of i th set of particles in a multimodal suspension
V_L	Volume of suspending medium of a multimodal suspension
V_n	Volume of n th set of particles in a multimodal suspension
V_N	Volume of largest-size particles in a multimodal suspension

References

1. Pal, R. *Rheology of Particulate Dispersions and Composites*; CRC Press: Boca Raton, FL, USA, 2007.
2. Pal, R. *Electromagnetic, Mechanical, and Transport Properties of Composite Materials*; CRC Press: Boca Raton, FL, USA, 2015.
3. Stickel, J.J.; Powell, R.L. Fluid mechanics and rheology of dense suspensions. *Annu. Rev. Fluid Mech.* **2005**, *37*, 127–149. [[CrossRef](#)]

4. Denn, M.M.; Morris, J.F. Rheology of non-Brownian suspensions. *Annu. Rev. Chem. Biomol. Eng.* **2014**, *5*, 203–228. [[CrossRef](#)] [[PubMed](#)]
5. Guazzelli, E.; Pouliquen, O. Rheology of dense granular suspensions. *J. Fluid. Mech.* **2018**, *852*, P1. [[CrossRef](#)]
6. Tadros, T.F. *Suspension Concentrates: Preparation, Stability and Industrial Applications*; De Gruyter: Berlin, Germany; Boston, MA, USA, 2017.
7. Schramm, L.L. *Emulsions, Foams, Suspensions, and Aerosols: Microscience and Applications*; Wiley-VCH Verlag: Weinheim, Germany, 2014.
8. Kulshreshtha, A.; Wall, M. *Pharmaceutical Suspensions: From Formulation Development to Manufacturing*; Springer: London, UK, 2010.
9. Halloran, J.W.; Tomeckova, V. Flow behavior of polymerizable ceramic suspensions as function of ceramic volume fraction and temperature. *J. Eur. Ceram. Soc.* **2011**, *31*, 2535–2542.
10. Camargo, I.L.; Morais, M.M.; Fortulan, C.A.; Branciforti, M.C. A review on the rheological behavior and formulations of ceramic suspensions for vat polymerization. *Ceram. Int.* **2021**, *47*, 11906–11921. [[CrossRef](#)]
11. Zhou, W.; Li, D.; Wang, H. A novel aqueous ceramic suspension for ceramic stereolithography. *Rapid Prototyp. J.* **2010**, *16*, 29–35. [[CrossRef](#)]
12. Pal, R. Modeling the viscosity of concentrated nanoemulsions and nanosuspensions. *Fluids* **2016**, *1*, 11. [[CrossRef](#)]
13. Einstein, A. Eine neue Bestimmung der Molekuldimension. *Ann. Phys.* **1906**, *19*, 289–306. [[CrossRef](#)]
14. Einstein, A. Berichtigung zumeiner Arbeit: Eine neue Bestimmung der Molekuldimension. *Ann. Phys.* **1911**, *34*, 591–592. [[CrossRef](#)]
15. Batchelor, G.K. Effect of Brownian motion on bulk stress in a suspension of spherical particles. *J. Fluid Mech.* **1977**, *83*, 97–117. [[CrossRef](#)]
16. Brady, J.F.; Bossis, G. Stokesian dynamics. *Ann. Rev. Fluid Mech.* **1988**, *20*, 111–157. [[CrossRef](#)]
17. Ladd, A.J.C. Hydrodynamic transport coefficients of random dispersions of hard spheres. *J. Chem. Phys.* **1990**, *93*, 3483–3494. [[CrossRef](#)]
18. Wang, G.; Fiore, A.M.; Swan, J.W. On the viscosity of adhesive hard sphere dispersions: Critical scaling and the role of rigid contacts. *J. Rheol.* **2019**, *63*, 229–245. [[CrossRef](#)]
19. Taylor, G.I. The viscosity of a fluid containing small drops of another liquid. *Proc. R. Soc. Lond. A* **1932**, *138*, 41–48.
20. Vand, V. Viscosity of solutions and suspensions. I. Theory. *J. Phys. Colloid Chem.* **1948**, *52*, 277–299. [[CrossRef](#)]
21. Vand, V. Viscosity of solutions and suspensions. II. Experimental determination of the viscosity-concentration function of spherical inclusions. *J. Phys. Colloid Chem.* **1948**, *52*, 300–314. [[CrossRef](#)]
22. Ward, S.G.; Whitmore, R.L. Studies of the viscosity and sedimentation of suspensions Part 1.—The viscosity of suspension of spherical particles. *Br. J. Appl. Phys.* **1950**, *1*, 286–290. [[CrossRef](#)]
23. Saito, N. Concentration dependence of the viscosity of high polymer solutions. *J. Phys. Soc.* **1950**, *5*, 4–8. [[CrossRef](#)]
24. Mooney, M. The viscosity of a concentrated suspension of spherical particles. *J. Colloid Sci.* **1951**, *6*, 162–170. [[CrossRef](#)]
25. Roscoe, R. The viscosity of suspensions of rigid spheres. *Br. J. Appl. Phys.* **1952**, *3*, 267–269. [[CrossRef](#)]
26. Brinkman, H.C. The viscosity of concentrated suspensions and solutions. *J. Chem. Phys.* **1952**, *20*, 571–581. [[CrossRef](#)]
27. Simha, R. A treatment of the viscosity of concentrated suspensions. *J. Appl. Phys.* **1952**, *23*, 1020–1024. [[CrossRef](#)]
28. Oldroyd, J.G. The elastic and viscous properties of emulsions and suspensions. *Proc. R. Soc. Lond. A* **1953**, *218*, 122–132.
29. Manley, R.S.J.; Mason, S.G. The viscosity of suspensions of spheres: A note on the particle interaction coefficient. *Can. J. Chem.* **1954**, *32*, 763–767. [[CrossRef](#)]
30. Van der Waarden, M. Viscosity and electroviscous effect of emulsions. *J. Colloid Sci.* **1954**, *9*, 215–222. [[CrossRef](#)]
31. Maron, S.H.; Pierce, P.E. Application of Ree-Eyring generalized flow theory to suspensions of spherical particles. *J. Colloid Sci.* **1956**, *11*, 80–95. [[CrossRef](#)]
32. Happel, J. Viscosity of suspensions of uniform spheres. *J. Appl. Phys.* **1957**, *28*, 1288–1292. [[CrossRef](#)]
33. Ting, A.P.; Luebbbers, R.H. Viscosity of suspensions of spherical and other isodimensional particles in liquids. *AIChE J.* **1957**, *3*, 111–116. [[CrossRef](#)]
34. Krieger, I.M.; Dougherty, T.J. Mechanism for non-Newtonian flow in suspensions of rigid particles. *Trans. Soc. Rheol.* **1959**, *3*, 137–152. [[CrossRef](#)]
35. Rutgers, R. Relative viscosity of suspensions of rigid spheres in Newtonian liquids. *Rheol. Acta* **1962**, *2*, 202–210. [[CrossRef](#)]
36. Thomas, D.G. Transport characteristics of suspensions: VIII. A note on the viscosity of Newtonian suspensions of uniform spherical particles. *J. Colloid Sci.* **1965**, *20*, 267–277.
37. Frankel, N.A.; Acrivos, A. On the viscosity of a concentrated suspension of solid spheres. *Chem. Eng. Sci.* **1967**, *22*, 847–853. [[CrossRef](#)]
38. Chong, J.S.; Christiansen, E.B.; Baer, A.D. Rheology of concentrated suspensions. *Trans. Soc. Rheol.* **1968**, *12*, 281–301. [[CrossRef](#)]
39. Lewis, T.B.; Nielsen, L.E. Viscosity of dispersed and aggregated suspensions of spheres. *J. Rheol.* **1968**, *12*, 421–443. [[CrossRef](#)]
40. Batchelor, G.K.; Green, J.T. The determination of the bulk stress in a suspension of spherical particles to order c^2 . *J. Fluid Mech.* **1972**, *56*, 401–427. [[CrossRef](#)]
41. Yaron, I.; Gal-Or, B. On viscous flow and effective viscosity of concentrated suspensions and emulsions. *Rheol. Acta* **1972**, *11*, 241–252. [[CrossRef](#)]

42. Smith, J.H. Rheology of Concentrated Suspensions of Spheres. Ph.D. Thesis, California Institute of Technology, Pasadena, CA, USA, 1972.
43. Jeffrey, D.J.; Acrivos, A. The rheological properties of suspensions of rigid particles. *AIChE J.* **1976**, *22*, 417–432. [[CrossRef](#)]
44. Quemada, D. Rheology of concentrated disperse systems and minimum energy dissipation principle: 1. Viscosity-concentration relationship. *Rheol. Acta* **1977**, *16*, 82–94. [[CrossRef](#)]
45. Graham, A.L. On the viscosity of suspensions of solid spheres. *Appl. Sci. Res.* **1981**, *37*, 275–286. [[CrossRef](#)]
46. Graham, A.L.; Bird, R.B. Particle clusters in concentrated suspensions. 1. Experimental observations of particle clusters. *Ind. Eng. Chem. Fundam.* **1984**, *23*, 406–410. [[CrossRef](#)]
47. Metzner, A.B. Rheology of Suspensions in Polymeric Liquids. *J. Rheol.* **1985**, *29*, 739–775. [[CrossRef](#)]
48. Poslinski, A.J.; Ryan, M.E.; Gupta, R.K.; Seshadri, S.G.; Frechette, F.J. Rheological behavior of filled polymeric systems I. Yield stress and shear-thinning effects. *J. Rheol.* **1988**, *32*, 703–735. [[CrossRef](#)]
49. Poslinski, A.J.; Ryan, M.E.; Gupta, R.K.; Seshadri, S.G.; Frechette, F.J. Rheological behavior of filled polymeric systems II. The effect of a bimodal size distribution of particulates. *J. Rheol.* **1988**, *32*, 751–771.
50. Pal, R.; Rhodes, E. Viscosity/concentration relationships for emulsions. *J. Rheol.* **1989**, *33*, 1021–1045. [[CrossRef](#)]
51. Park, M.; Gandhi, K.; Sun, L.; Salovey, R. Model-filled polymers. III: Rheological behavior of polystyrene containing cross-linked polystyrene beads. *Polym. Sci. Eng.* **1990**, *30*, 1158–1164.
52. Jones, A.A.R.; Leary, B.; Boger, D.V. The rheology of a concentrated colloidal suspension of hard spheres. *J. Colloid Interface Sci.* **1991**, *147*, 479–495. [[CrossRef](#)]
53. Jones, A.A.R.; Leary, B.; Boger, D.V. The rheology of a sterically stabilized suspension at high concentration. *J. Colloid Interface Sci.* **1992**, *150*, 84–96. [[CrossRef](#)]
54. Ilic, V.; Phan-Thien, N. Viscosity of concentrated suspensions of spheres. *Rheol. Acta* **1994**, *33*, 283–291. [[CrossRef](#)]
55. Pal, R. Rheology of emulsions containing polymeric liquids. In *Encyclopedia of Emulsion Technology*; Chapter, 3, Becher, P., Eds.; Dekker: New York, NY, USA, 1996; Volume 4.
56. Weiss, A.; Dingenouts, N.; Ballauff, M.; Senf, H.; Richtering, W. Comparison of the effective radius of sterically stabilized latex particles determined by small angle X-ray scattering and by zero shear viscosity. *Langmuir* **1998**, *14*, 5083–5087. [[CrossRef](#)]
57. Pal, R. Linear viscoelastic behavior of multiphase dispersions. *J. Colloid Interface Sci.* **2000**, *232*, 50–63. [[CrossRef](#)]
58. Zarraga, I.E.; Hill, D.A.; Leighton, D.T. The characterization of the total stress of concentrated suspensions of noncolloidal spheres in Newtonian fluids. *J. Rheol.* **2000**, *44*, 185–220. [[CrossRef](#)]
59. Pal, R. Evaluation of theoretical viscosity models for concentrated emulsions at low capillary numbers. *Chem. Eng. J.* **2001**, *81*, 15–21. [[CrossRef](#)]
60. Pal, R. Novel viscosity equations for emulsions of two immiscible liquids. *J. Rheol.* **2001**, *45*, 509–520. [[CrossRef](#)]
61. Pal, R. Complex shear modulus of concentrated suspensions of solid spherical particles. *J. Colloid Interface Sci.* **2002**, *245*, 171–177. [[CrossRef](#)] [[PubMed](#)]
62. Pal, R. A new linear viscoelastic model for emulsions and suspensions. *Poly. Eng. Sci.* **2008**, *48*, 1250–1253. [[CrossRef](#)]
63. Mendoza, C.I.; Santamaria-Holek, I. The rheology of hard sphere suspensions at arbitrary volume fractions: An improved differential viscosity model. *J. Chem. Phys.* **2009**, *130*, 044904.
64. Brouwers, H.J.H. Viscosity of a concentrated suspension of rigid monosized particles. *Phys. Rev. E* **2010**, *81*, 051402. [[CrossRef](#)]
65. Pal, R. Rheology of simple and multiple emulsions. *Curr. Opin. Coll. Interface Sci.* **2011**, *16*, 41–60. [[CrossRef](#)]
66. Tanner, R.I.; Qi, F.; Dai, S. Scaling the normal stresses in concentrated non-colloidal suspensions of spheres. *Rheol. Acta* **2013**, *52*, 291–295. [[CrossRef](#)]
67. Pal, R. New models for the viscosity of nanofluids. *J. Nanofluids* **2014**, *3*, 260–266. [[CrossRef](#)]
68. Pal, R. Rheology of suspensions of solid particles in power-law fluids. *Can. J. Chem. Eng.* **2015**, *93*, 166–173. [[CrossRef](#)]
69. Pal, R. A new model for the viscosity of asphaltene solutions. *Can. J. Chem. Eng.* **2015**, *93*, 747–755. [[CrossRef](#)]
70. Faroughi, S.A.; Huber, C. A generalized equation for rheology of emulsions and suspensions of deformable particles subjected to simple shear at low Reynolds number. *Rheol. Acta* **2015**, *54*, 85–108. [[CrossRef](#)]
71. Pal, R. Viscosity-concentration relationships for nanodispersions based on glass transition point. *Can. J. Chem. Eng.* **2017**, *95*, 1605–1614. [[CrossRef](#)]
72. Pal, R. New generalized viscosity model for non-colloidal suspensions and emulsions. *Fluids* **2020**, *5*, 150. [[CrossRef](#)]
73. Cheng, Z.; Zhu, J.; Chaikin, P.M.; Phan, S.E.; Russel, W.B. Nature of dicergence in low shear viscosity of colloidal hard-sphere dispersions. *Phys. Rev. E* **2002**, *65*, 041405. [[CrossRef](#)]
74. Boyer, F.; Guazzelli, E.; Pouliquen, O. Unifying suspension and granular rheology. *Phys. Rev. Lett.* **2011**, *107*, 188301. [[CrossRef](#)]
75. Wilms, P.; Hinrichs, J.; Kohlus, R. Macroscopic rheology of non-Brownian suspensions at high shear rates: The influence of solid volume fraction and non-Newtonian behaviour of the liquid phase. *Rheol. Acta* **2022**, *61*, 123–138.
76. De Kruif, C.G.; Van Lersel, E.M.F.; Vrij, A.; Russel, W.B. Hard sphere colloidal dispersions: Viscosity as a function of shear rate and volume fraction. *J. Chem. Phys.* **1985**, *83*, 4717–4725.
77. Van der Werff, J.C.; De Kruif, C.J. Hard-sphere colloidal dispersions: The scaling of rheological properties with particle size, volume fraction, and shear rate. *J. Rheol.* **1989**, *33*, 421–454.
78. Rodriguez, B.E.; Kaler, E.W.; Wolfe, M.S. Binary mixtures of monodisperse latex dispersions. *Viscosity. Langmuir* **1992**, *8*, 2382–2389. [[CrossRef](#)]

79. Shikata, T.; Pearson, D.S. Viscoelastic behavior of concentrated spherical suspensions. *J. Rheol.* **1994**, *38*, 601–616. [[CrossRef](#)]
80. Nguyen, C.T.; Desgranges, F.; Roy, G.; Galanis, N.; Mare, T.; Boucher, S.; Angue Mintsa, H. Temperature and particle-size dependent viscosity data for water-based nanofluids-hysteresis phenomenon. *Int. J. Heat Fluid Flow* **2007**, *28*, 1492–1506. [[CrossRef](#)]
81. Nguyen, C.T.; Desgranges, F.; Galanis, N.; Roy, G.; Mare, T.; Boucher, S.; Angue Mintsa, H. Viscosity data for Al₂O₃ nanofluid-hysteresis: Is heat transfer enhancement using nanofluids reliable? *Int. J. Therm. Sci.* **2008**, *47*, 103–111.
82. Ghanaatpishehsanaei, G.; Pal, R. Rheology of suspensions of solid particles in liquids thickened by starch nanoparticles. *Colloids Interfaces* **2023**, *7*, 52. [[CrossRef](#)]
83. Tanner, R.I. Review Article: Aspects of non-colloidal suspension rheology. *Phys. Fluids* **2018**, *30*, 101301.
84. Morris, J.F. Shear thickening of concentrated suspensions: Recent developments and relation to other phenomenon. *Ann. Rev. Fluid Mech.* **2020**, *52*, 121–144.
85. Farris, R.J. Prediction of the viscosity of multimodal suspensions from unimodal viscosity data. *J. Rheol.* **1968**, *12*, 281–301. [[CrossRef](#)]

Disclaimer/Publisher's Note: The statements, opinions and data contained in all publications are solely those of the individual author(s) and contributor(s) and not of MDPI and/or the editor(s). MDPI and/or the editor(s) disclaim responsibility for any injury to people or property resulting from any ideas, methods, instructions or products referred to in the content.